Generation and attenuation of variability in a bacterial signaling network revealed by single-cell FRET

J.M. Keegstra[1], **K. Kamino**[1], **F. Anquez §**[1], **M.D. Lazova**[1], **T. Emonet**[2], **T.S. Shimizu**[1]

***For correspondence:** t.shimizu@amolf.nl (TSS)

Present address: §University of Lille, France

[1]AMOLF Institute, Science Park 104, 1098XG Amsterdam, the Netherlands; [2]Department of Cellular and Molecular Biology, Yale University, New Haven, USA

Abstract We present *in vivo* single-cell FRET measurements in the *Escherichia coli* chemotaxis system that reveal the influence of network design on noise-induced variability, both across cells in isogenic populations and within individual cells over time. We find pervasive cell-to-cell variability in ligand-response sensitivity, adaptation timescale, as well as the steady-state set point of network output, and analyze the role of network parameters and topology in shaping this diversity. In the absence of ligand stimulation or changes in gene expression, we observe temporal fluctuations in the intracellular signal attributable to stochastic activities of adaptation enzymes CheR and CheB, with unexpectedly large amplitudes (>2-fold previous estimates). Our results demonstrate how signaling networks can tune population diversity and temporal variability by either amplifying or suppressing molecular noise, arising not only in gene expression processes but also in stochastic protein-protein interactions.

Introduction

Cellular physiology is deeply shaped by molecular fluctuations, resulting in phenotypic variability that can be both detrimental and beneficial (**Rao et al., 2002**). One of the most important and well-studied sources of intracellular fluctuations is stochastic gene expression (**Elowitz et al., 2002**; **Eldar and Elowitz, 2010**; **Raj and Van Oudenaarden, 2008**), which can generate substantial cell-to-cell variability in protein levels within isogenic populations under invariant environmental conditions. Such heterogeneity in protein counts are readily measurable by fluorescent-protein reporters (**Elowitz et al., 2002**; **Ozbudak et al., 2002**) , but mechanistically tracing the consequences of such molecular noise to the level of complex cellular phenotypes such as signaling and motility remains a significant challenge, in part due to the multitude of interactions between gene products, but also because each of those interactions can, in principle, become an additional source of noise. In this paper, we study how multiple sources of molecular noise, arising in both gene expression and protein-protein interactions, affect performance of the *E. coli* chemotaxis network, a canonical signaling pathway.

In bacteria, gene-expression noise tends to manifest itself as stable cell-to-cell differences in phenotypes that persist over the cell's generation time, because typical protein lifetimes are longer than the cell cycle (**Li et al., 2014**). The architecture of signaling networks can have a profound influence on their sensitivity to such noise-induced differences in protein levels, and it has been shown that the design of the *E. coli* chemotaxis network confers robustness of a number of signaling parameters, such as precision of adaptation, against variability in gene expression (**Barkai and Leibler, 1997**; **Kollmann et al., 2005**). On the other hand, cell-to-cell differences in behavior can also be advantageous for isogenic populations under uncertain and/or time-varying environments, and it has been argued that the manner in which the chemotaxis network filters gene expression noise to shape phenotype distributions could be under selective pressure (**Frankel et al., 2014**; **Waite et al., 2016**).

In principle, molecular noise arising in processes other than gene expression, such as protein-protein interactions within signaling pathways, can also contribute to cellular variability. However, such noise sources tend to be harder to study experimentally because, in contrast to gene-expression noise, which can be characterized by measuring fluorescent reporter levels (**Elowitz et al., 2002**; **Raser and O'Shea, 2004**), requirements for *in vivo* measurements of protein-protein interactions tend to be more demanding and no generically applicable strategies exist. The *E. coli* chemotaxis system provides a compelling experimental paradigm for addressing protein-signaling noise, because a powerful technique for *in vivo* measurements of protein signaling, based on Förster resonance energy transfer (FRET), has been successfully developed (**Sourjik and Berg, 2002b**; **Sourjijk et al., 2007**).

The chemotaxis network controls the motile behavior of *E. coli*, a run-and-tumble random

walk that is biased by the signaling network to achieve net migrations toward favorable directions. The molecular mechanisms underlying this pathway have been studied extensively (for recent reviews, see refs. ***Wadhams and Armitage*** (***2004***); ***Tu*** (***2013***); ***Parkinson et al.*** (***2015***)). In brief, transmembrane chemoreceptors bind to ligand molecules, inhibiting the autophosphorylation of a central kinase, CheA. When active, CheA transfers its phosphate to CheY to form CheY-P. Meanwhile, the phosphatase CheZ degrades CheY-P to limit the signal lifetime. CheY-P binds to a flagellar motor, which in turn increases the chance of the motor to turn clockwise, leading to a tumble. An adaptation module consisting of the enzymes CheR and CheB implements negative integral feedback by tuning the sensitivity of the chemoreceptors via reversible covalent modifications that restore the kinase activity (and CheY-P level).

Despite its relative simplicity, this pathway exhibits many interesting network-level functionalities, such as cooperative signal amplification (***Segall et al., 1986***; ***Sourjik and Berg, 2002b***; ***Bray et al., 1998***), sensory adaptation (***Barkai and Leibler, 1997***; ***Alon et al., 1999***) and fold-change detection (***Mesibov et al., 1973***; ***Lazova et al., 2011***), and FRET microscopy has proven extremely powerful in characterizing such signal processing of the chemotaxis pathway, especially in *E. coli* (***Sourjik and Berg, 2002b***, ***2004***; ***Shimizu et al., 2010***; ***Oleksiuk et al., 2011***), but also in Salmonella (***Lazova et al., 2012***) and *B. subtilis* (***Yang et al., 2015***). It has been implemented in various ways (***Sourjik and Berg, 2002b***,a; ***Shimizu et al., 2006***; ***Kentner and Sourjik, 2009***), but most commonly by using CFP and YFP as the FRET donor-acceptor pair, fused to CheY and CheZ, respectively. To date, however, nearly all applications of FRET in the bacterial chemotaxis system have been population-level measurements in which signals from hundreds to thousands of cells are integrated to achieve a high signal-to-noise ratio. A pioneering study applied FRET at the single-cell level to study spatial heterogeneities in CheY-CheZ interactions (***Vaknin and Berg, 2004***), but those measurements were limited to relatively short times due to phototoxicity and bleaching.

By exploring a range of fluorescent proteins as FRET pairs, and improving measurement protocols, we have developed a robust method for single-cell FRET measurements of chemotactic signaling dynamics in single bacteria over extended times. The data reveal extensive cell-to-cell variability, as well as temporal fluctuations that are masked in population-level FRET measurements. In contrast to previous single-cell experiments that relied on measurements of motor output or swimming behavior (***Berg and Brown, 1972***; ***Spudich and Koshland, 1976***; ***Segall et al., 1986***; ***Korobkova et al., 2004***; ***Park et al., 2010***; ***Masson et al., 2012***), FRET alleviates the need to make indirect inferences about intracellular molecular interactions through the highly noisy 2-state switching of the flagellar motor, whose response function can vary over time due to adaptive remodeling (***Yuan et al., 2012***). In a typical experiment, we are able to obtain dozens of (up to ~100) single-cell FRET time series simultaneously, to efficiently collect statistics of phenotypic and temporal variability.

Results

Single-cell FRET reveals pervasive cell-to-cell variability in intracellular signaling

To measure variability in intracellular signaling, we adapted a FRET assay for chemotaxis widely used for population-level measurements with fluorescent fusions to CheY and its phosphatase CheZ (***Sourjik and Berg, 2002b***). On timescales longer than the relaxation of CheY's phosphorylation/dephosphorylation cycle, the FRET level reflects the phosphorylation rate of CheY by the CheA kinase, thus providing an efficient *in vivo* measurement of the network activity (Fig. S1). Instead of the conventional CFP/YFP FRET pair we used the fluorophores YFP and mRFP1 to avoid excitation with blue light, which induces considerably stronger photoxicity and also perturbs the chemotaxis system as a repellent stimulus (***Taylor and Koshland, 1975***; ***Taylor et al., 1979***; ***Wright et al., 2006***). A field of *E. coli* cells expressing this FRET pair were immobilized on a glass surface imaged in two fluorescence channels, and segmented offline to compute a FRET time series for each cell in the field of view (see Materials and Methods).

For wild-type cells (Fig. 1a) we found that the ensemble mean of single-cell FRET responses, $\langle \mathrm{FRET} \rangle(t)$, agrees well with previous population-level measurements (***Sourjik and Berg, 2002b***). Upon prolonged stimulation with a saturating dose of attractant α-methylaspartate (MeAsp), $\langle \mathrm{FRET} \rangle(t)$ rapidly fell to zero before gradually returning to the pre-stimulus level due to adaptation. Upon removal of attractant, $\langle \mathrm{FRET} \rangle(t)$ rapidly increased to a maximum before returning to the pre-stimulus baseline. Single-cell FRET time series, $\mathrm{FRET}_i(t)$, had qualitatively similar profiles, but the kinetics of adaptation and response amplitudes demonstrate differences from cell to cell. For each cell, $\mathrm{FRET}_i(t)$ is limited by the slow autophosphorylation of CheA and hence is proportional to $a[\mathrm{CheA}]_{\mathrm{T},i}$ (provided [CheY] and [CheZ] are sufficiently high, see Materials and Methods), in which a is the activity per kinase and $[\mathrm{CheA}]_{\mathrm{T},i}$ the total amount of kinases part of the receptor-kinase complex. Hence from the $\mathrm{FRET}_i(t)$ the activity per kinase a can be readily determined by normalizing each FRET timeseries by its maximum response $a = \mathrm{FRET}_i/\mathrm{FRET}_{i,\mathrm{max}}$ (Figure 1b). The steady-state activity $a_{0,i}$ is then defined as the activity before the addition of attractant. The baseline activity per cell varies from cell-to-cell a_0 (Fig. 1b, CV=0.22). The network activity controls the flagellar motor rotation, and hence this is consistent with the observation that cells in isogenic population exhibit a variable steady-state tumble frequency (***Spudich and Koshland, 1976***; ***Dufour et al., 2016***).

The adaptation precision is defined as its post-adaptational activity level ($\Pi = a_{adapted,i}/a_{0,i}$), hence a precision of 1 refers to perfect adaptation. The adaptation kinetics are quantified by the recovery time, the time required for each cell to recover to 50% of its post-adaptational activity level ($a_{adapted,i}$). When observing the distributions of these parameters we noted that the cell-to-cell variability (quantified by the coefficient of variation CV), is high in the precision Π (Fig. 1d, CV=0.40) but the average precision (0.79) agrees well with population measurements (***Neumann et al., 2014***). The variation is also substantial in $\tau_{recovery}$ (Fig. 1d, CV=0.20). This falls within the range of ~20-50%

from previous reports, in which single-cell recovery times were estimated from motor-rotation or swimming-behavior measurements (***Berg and Tedesco, 1975***; ***Spudich and Koshland, 1976***; ***Min et al., 2012***). The time required to recover from a saturating amount of attractant is determined not only by the stimulus size, but also the methylation rate of receptor modification sites catalyzed by CheR and the number of such sites that need to be methylated. Variability in the recovery time is thus likely to reflect cell-to-cell variability in the ratio between the expression level of CheR and that of the chemoreceptor species responding to ligand (Tar for the experiment in Fig. 1a).

Thus, single-cell FRET allows efficient measurement of single-cell signaling dynamics that, on average, agree well with previous population-level FRET experiments and single-cell flagellar-based experiments, thereby revealing variability in a wide variety of signaling parameters.

Diversity in the ligand response is modulated during population growth

The chemotactic response of *E. coli* to chemoeffectors is known to be highly sensitive, with receptor-occupancy changes of less than 1% eliciting detectable responses both at the level of flagellar motor rotation (***Segall et al., 1986***) and the intracellular signal (***Sourjik and Berg, 2002b***). Naively, one might expect variability to be detrimental for sensory performance, and conversely that a highly sensitive system would imply less variability. Indeed, at the population level, the greatest apparent gain in the response (defined as the fractional change in output divided by fractional change in input) is observed in adaptation-deficient (CheRB-) cells, in which the receptor population is homogeneous with respect to their adaptational modification state.

We probed the ligand sensitivity of CheRB- cells (TSS58) at the single-cell level by FRET dose-response measurements in which step stimuli of successively larger amplitudes were applied over time (Fig. 2). Considerable variability in the response to the attractant L-serine were observed across the population of immobilized cells simultaneously experiencing the same stimulus, with response magnitudes often ranging from virtually zero to full response (Fig. 2a). The resulting dose-response data were analyzed by fitting each individual cell's FRET response by a Hill curve of the form $[1 + ([L]/K)^H]^{-1}$, where the parameters K and H are defined as the sensitivity and steepness, respectively, of the response. The family of dose response curves constructed from this ensemble of fit parameters reveals considerable variability from cell to cell in the shape of the response curve (Fig. 2b).

What could be the cause of the diversity in ligand response in the absence of adaptation-induced heterogeneity? We reasoned that expression-level variability of the five chemoreptor species of *E. coli*, which are known to form mixed clusters with cooperative interactions (***Ames et al., 2002***; ***Sourjik and Berg, 2004***), could endow isogenic populations with sensory diversity. In line with this idea, CheRB- cells expressing only a single chemoreceptor species (Tsr) demonstrated not only higher cooperativity, but also attenuated variability in the dose-response profile from cell to cell (Figure 2b-c), showing that the composition of the receptor population is important not only to

tune the average ligand response of a population, but also in generating a wide range of sensory phenotypes within an isogenic population.

It has been shown that expression level of chemoreceptors changes during growth of *E. coli* batch cultures: concomitant with the slowing of growth upon the transition from the exponential phase towards early stationary phase, the relative expression level ratio Tar/Tsr increases from majority Tsr (Tar/Tsr< 1) to majority Tar (Tar/Tsr> 1) (***Salman and Libchaber, 2007***; ***Kalinin et al., 2010***). To probe the consequence of such changes for ligand-sensing diversity, we measured single-cell dose response curves in populations harvested at different cell densities during batch growth (Figure 2d). The resulting population-averaged responses show a dependence of dose-response parameters on the optical density (O.D.) of the culture, shifting from highly sensitive (low K) and highly cooperative (high H) at low cell densities (OD≈ 0.3) to less sensitive (high K) and less cooperative (low H) at increased cell densities (OD≈ 0.45, and OD ≈ 0.6) (Fig. 2d, open triangles, and Fig. S6). This trend is also visible at the level of single cells, but we found the responses to be highly variable under each condition (Fig. 2d, filled points). Remarkably, both sensitivity K and cooperativity H varied by over an order of magnitude, far exceeding the uncertainty in parameter estimates due to experimental noise (Fig. S7).

To further test the idea that ligand-response diversity is governed by differences in receptor expression levels, we considered the pattern of covariation between the fitted sensitivity K and cooperativity H in single cells (Figure 2b, blue). In contrast to cells expressing Tsr as the only chemoreceptor, in which the variability in K is only 20 $\%$ (Figure 2b, orange), single cells expressing a wildtype complement of chemoreceptors demonstrated strong variation in K. This variation was negatively correlated with the cooperativity H (Figure 2d). Noting that this overall pattern of covariation agrees well with dose response parameters obtained from population-level FRET experiments in which the Tar/Tsr ratio was experimentally manipulated via plasmid-based expression control (Figure 2d, open triangles; data from ***Sourjik and Berg*** (***2004***)), we proceeded to quantitatively estimate the diversity in the Tar/Tsr ratio via fits of a multi-species MWC model (***Mello and Tu, 2005***; ***Keymer et al., 2006***) to single-cell FRET data (see Materials and Methods). The resulting distribution of single-cell Tar/Tsr estimates (Figure 2e) was dominated by Tsr in cells harvested early (OD≈ 0.3) but the relative contribution of Tar increased in cells harvested at later stages of growth (OD≈ 0.45 and OD≈ 0.6). Interestingly, in addition to this increase in the mean of the Tar/Tsr distribution during batch growth, which confirms previous reports that found increased Tar/Tsr ratios at the population level (***Salman and Libchaber, 2007***; ***Kalinin et al., 2010***), we find that the breadth of the distribution also increases at later stages of growth. Thus, modulation of receptor expression during growth provides a means of tuning not only response sensitivity and cooperativity, but also single-cell diversity in the response of cell populations experiencing identical changes in their common environment.

The large variability in the Tar/Tsr ratio ($CV \approx 0.5$ at O.D.=0.45) is somewhat surprising given that

the mean expression level of both receptors are known to be high and of order 10^3-10^4 copies per cell (***Li and Hazelbauer, 2004***). At such high expression, intrinsic noise in expression levels (i.e. due to the production and degradation process of proteins, expected to scale as the square root of the mean) could be as low as a few percent of the mean, and gene-expression fluctuations are expected to be dominated by extrinsic noise components (i.e. those affecting regulation of gene expression, which do not scale with the mean). In *E. coli*, a global survey of gene expression noise established an empirical lower bound to extrinsic noise at $CV \approx 0.3$ (***Taniguchi et al., 2010***), and measurements within the chemotaxis system also indicate that between a subset of chemotaxis genes, the extrinsic component of covariation does approach this limit (***Kollmann et al., 2005***). Interestingly, however, in a recent study (***Yoney and Salman, 2015***) found using single-cell flow-cytometry a high degree of variability in the ratio of Tar/Tsr promotor activities ($CV \approx 0.45$ at O.D.=0.51) comparable to the range of ratios extracted from our analysis of dose response data. Given that cell-to-cell variability in the Tar/Tsr ratio is much greater than achievable lower bounds of gene-expression noise in bacteria, it would be interesting to investigate the mechanistic sources of this variability, such as operon organization, RBS strength, and promotor stochasticity (***Frankel et al., 2014***).

Variability in receptor expression could also explain the distribution of adaptation precision we observed in wildtype cells (Figure 1d). In a previous population-level study, it has been shown that adaptation precision depends strongly on the expression-level ratio between the multiple chemoreceptor species, with the highest adaptation precision being achieved when the ligand-binding receptor is a minority within the total receptor population (***Neumann et al., 2014***). Thus, the substantial heterogeneity in adaptation precision we observed (CV = 0.40) upon a saturating MeAsp stimulus is consistent with strong variability in the Tar/Tsr ratio.

CheB phosphorylation feedback attenuates cell-to-cell variability

While bacteria can exploit molecular noise for beneficial diversification, variability can also limit reliable information transfer and degrade sensory performance. In the framework of *E. coli*'s run-and-tumble navigation strategy, chemotactic response to gradients requires that cells maintain a finite tumble bias (*i.e.* avoiding extreme values zero and one), to suppress unresponsive phenotypes that fail to switch between run and tumble states in response to the environmental inputs. One important mechanism that ensures responsiveness to stimuli over a broad range of input levels is sensory adaptation mediated by the methyltransferase/methylesterase pair CheR/CheB. These receptor-modifying enzymes provide negative feedback through the dependence of their catalytic activity on the receptor's signaling state: the rate of methylation (demethylation) by CheR (CheB) is a decreasing (increasing) function of receptor-kinase activity (***Borczuk et al., 1986***; ***Amin and Hazelbauer, 2010***). This dependence of enzyme activity on the substrate conformation provides negative integral feedback that ensures precise adaptation (***Barkai and Leibler, 1997***) toward the pre-stimulus steady-state activity a_0.

Interestingly, one of the two adaptation enzymes, CheB, can be phosphorylated by CheA, the kinase whose activity it controls through its catalytic (demethylation) activity on receptors. Effectively, this adds an additional negative feedback loop to the network, but the role of this phosphorylation-dependent feedback has remained elusive since it has been shown to be dispensable for precise adaptation (***Alon et al., 1999***). Through theoretical analysis, it has been conjectured that this secondary feedback loop might play a role in attenuating effects of gene-expression noise (***Kollmann et al., 2005***), but experimental verification has been lacking. We therefore sought to investigate the influence of perturbations to this network topology on the variability of chemotactic signaling activity.

CheB consists of two domains connected by a flexible linker (Figure 3a). A regulatory domain, with structural similarity to CheY, can be phosphorylated at residue Asp^{56} (***Djordevic et al., 1998***; ***Stewart et al., 1990***). A catalytic domain mediates binding to specific residues on chemoreceptor cytoplasmic domains and removes a methyl group added by the counterbalncing activity of CheR. Phosphorylation induces a conformational change and activates CheB (CheB*) (***Djordevic et al., 1998***; ***Lupas and Stock, 1989***). Several mutants of CheB lack phosphorylation feedback while retaining catalytic activity. Here, we focus on two specific mutants: $CheB^{D56E}$, which bears a point mutation at the phosphorylation site, and $CheB_c$, which expresses only the catalytic domain of CheB (***Stewart et al., 1990***; ***Alon et al., 1999***). Cells expressing these mutants have an altered network topology (Figure 3b) which lacks CheB phosphorylation feedback.

To study the influence of network topology on cell-to-cell variability, we expressed different forms of CheB ($CheB^{WT}$, $CheB^{D56E}$, $CheB_c$) from an inducible promoter in a Δ*cheB* strain and measured the response to a saturating amount of attractant (500 μM MeAsp). The expression levels of each mutant are tuned such that they approximate the wild-type steady state activity level. The response of $CheB^{WT}$ was, as expected, very similar to cells in which CheB is expressed from its native chromosomal position (compare Figs. S9a and 1a). By contrast, cells expressing either of the two CheB mutants defective in phosphorylation demonstrated increased cell-to-cell variability in the steady-state activity compared to cells expressing $CheB^{WT}$. The increased variability of the CheB phosphorylation-deficient mutants ($CheB^{D56E}$ and $CheB_c$) was manifested not only in a higher coefficient of variation in a_0 (1.07 and 1.10, respectively, and WT 0.7), but also a qualitatively different shape of the distribution of a_0 across the population (Figure 3c). Whereas the distribution demonstrated a single peak in $CheB^{WT}$ cells with phosphorylation feedback, the distribution for the phosphorylation-feedback mutants demonstrated a bimodal shape with peaks close to the extreme values $a_0 = \{0, 1\}$.

We tested whether these strong differences in cell-to-cell variability might be the result of gene expression noise, by comparing expression-level distributions of the CheB mutants. We constructed fluorescent fusions of each *cheB* allele to the yellow fluorescent protein mVenus and quantified the distribution of single-cell fluorescence levels under the same induction conditions as in the FRET ex-

periments (figure S9). The ratio between the measured expression-levels (CheBc:WT:D56E≈0.7:1:2.5) was compatible with expectations from the hierarchy of reported *in vitro* rates ($k_b^{\mathrm{D56E}} < k_b^{WT} < k_b^{c}$) (**Anand and Stock, 2002**; **Simms et al., 1985**; **Stewart, 1993**), and expression-level variability, characterized by the coefficient of variation (CV), was very similar between the three strains (0.87,0.90 and 0.82). These findings suggest that the differences in cell-to-cell variability observed in FRET are not due to differences between the expression-level distributions of the three *cheB* alleles, but rather to the differences they impose on the signaling network topology.

What feature of the signaling network could generate such broad (and even bimodal) distributions of a_0? It has been conjectured (**Barkai and Leibler, 1997**; **Emonet and Cluzel, 2008**) and demonstrated (**Shimizu et al., 2010**) that *in vivo* the enzymes CheR and CheB operate at or near saturation. An important consequence of enzyme saturation in such reversible modification cycles is that the steady-state activity of the substrate becomes highly sensitive to the expression level ratio of the two enzymes, a phenomenon known as zero-order ultrasensitivity (**Goldbeter and Koshland (1981)**; see Materials and Methods). Within the chemotaxis system, saturation of both CheR and CheB can thus render the receptor modification level, and in turn, the CheA activity a_0, ultrasensitive to the [CheR]/[CheB] concentration ratio. If we view this ultrasensitive mapping as a transfer function f between the ratio [CheR]/[CheB] and the steady-state activity a_0,

$$a_0 = f([\mathrm{CheR}]/[\mathrm{CheB}])$$

then its characteristic steep sigmoidal profile can impose bimodality in the methylation level, and hence also in the activity of steady-state CheA activity, a_0, even at quite modest input variances for distributions of the ratio $P_{RB}([\mathrm{CheR}]/[\mathrm{CheB}])$. This is because the manner in which the transfer function f filters the [CheR]/[CheB] distribution,

$$P(a_0) = \frac{P_{RB}(f^{-1}(a_0))}{\left|f'(f^{-1}(a_0))\right|}.$$

spreads the narrow range in the [CheR]/[CheB] distribution $P_{RB}([\mathrm{CheR}]/[\mathrm{CheB}])$ over which $f([\mathrm{CheR}]/[\mathrm{CheB}])$ is steep across a broad range in a_0. Thus, even if expression-level noise for both CheR and CheB are modest, an ultrasensitive transfer function f can effectively amplify the variation in [CheR]/[CheB], and if the distribution of the latter ratio, $P_{RB}([\mathrm{CheR}]/[\mathrm{CheB}])$ extends below and above the narrow region over which f is steep, the decreased slope of f (i.e. lower $f'([\mathrm{CheR}]/[\mathrm{CheB}])$) in those flanking regions will tend to increase the weight on both sides of the broad $P(a_0)$ distribution to produce a bimodal profile. On the other hand, if the steepness of f is reduced, the resulting $P(a_0)$ will have a reduced variance for the same input $P_{RB}([\mathrm{CheR}]/[\mathrm{CheB}])$.

Could the known biochemical differences between the three forms of CheB ($\mathrm{CheB}^{\mathrm{WT}}$, $\mathrm{CheB}^{\mathrm{D56E}}$, CheB_c) explain the contrasting patterns of a_0 variability observed in our single-cell FRET experiments? In the absence of any feedback, the steepness of $f(CheR/CheB)$ is solely determined by the low

Michaelis-Menten constants $K_{B,R}$, which corresponds to saturated kinetics of the enzymatic activity of CheRB and hence ultransensitivity of the steady-state substrate activity. The expression ratio of CheR/CheB which determines the crossover point (a_0=0.5) is set by the ratio of catalytic rates of CheR and CheB ($k_{r,b}$). Hence the phosphorylation deficient mutants CheB^{D56E} and CheB$_c$ both have steep curves but are shifted along the R/B axis due to very different catalytic rates. However,in the case of phosphorylation feedback, CheB^{WT}, the same enzyme can be in two states, each with equal $K_{r,b}$ but one low and one high k_r. Whether CheB is in the one state or the other is determined by the activity-dependent phosphorylation feedback. As a result, the curve of CheB^{D56E} is activity dependent ($f(a, CheR/CheB)$) and changes with activity by shifting between the two curves corresponding to the extremes of all phosphorylated or all unphosphorylated. Effectively, this makes the resulting curve f less steep. The mean of the distributions P_{RB} are tuned such to get the same mean activity level ($\langle a_0 \rangle$), but the same variance in P_{RB} leads to very wide $P(a_0)$ distributions in absence of phosphorylation, while phosphorylation feedback ensures a much smaller, single-peaked distrubtion.

It has also been conjectured that the CheB phosphorylation feedback is responsible for the highly nonlinear kinetics of recovery from repellent (or attractant removal) responses ***Shimizu et al. (2010)***. Indeed, in cells expressing CheB$_c$, the kinetics of recovery from the response to removal of 500 μ MeAsp after adaptation appeared qualitatively different from that in cells expressing wildtype CheB, lacking the characteristic rapid recovery and instead appearing more symmetric with the CheR-mediated recovery upon addition of a saturating dose of attractant (Fig. S10). By contrast, CheB^{D56E} was found to still possesses a fast component, despite being defective in phosphorylation, albeit also with somewhat slower kinetcs than wt. In summary, the clearest difference between wildtype and phosphorylation-defective CheB mutants is found in the variability of the steady-state signal output (i.e. kinase activity).

The bimodal distribution in kinase activity we observed in the phosphorylation-deficient CheB mutants implies that a large fraction of cells have a CheY-P concentration far below or far above the motor's response threhold and hence will impair chemotactic responses to environmental gradients. Consistent with this idea, in motility-plate experiments (Supplementary Figure S11) we found that chemotactic migration on soft-agar plates was severely compromised for both CheB^{D56E} and CheB$_c$ compared to CheB$_{WT}$, indicating that the phosphorylation feedback is important for efficient collective motility.

Protein-signaling noise generates large temporal fluctuations in network output

The slow kinetics of the adaptation enzymes CheR and CheB have been hypothesized to play a role not only in determining the steady-state kinase activity a_0, but also in generating temporal fluctuations of the intracellular signal (***Korobkova et al., 2004***; ***Emonet and Cluzel, 2008***; ***Park et al., 2010***; ***Celani and Vergassola, 2012***). We found substantial differences between wildtype (CheRB+)

and adaptation-deficient (CheRB-) cells in the variability of their FRET signals across time (Fig. 4). The effect is clearly visible upon comparing long (~1h) FRET time series obtained from cells of these two genotypes (Figure 4a). The FRET signal in wildtype cells demonstrated transient excursions from the mean level that were far greater in amplitude than those in CheRB- cells. This amplitude $\eta \equiv \sigma_a/\langle a \rangle$ was quantified by computing the variance of each single-cell time series, low-pass filtered with a moving average filter of 10s, and shows that the fluctuation amplitudes are much larger in wildtype cells ($\langle \eta \rangle = 0.44$) compared to adaptation-deficient cells ($\langle \eta \rangle = 0.09$). Importantly, these experiments were carried out under conditions in which no protein synthesis can occur due to auxotrophic limiation (see Materials and Methods), thus ruling out gene-expression processes as the source of these fluctuations.

Power spectral density (PSD) estimates computed from such time series confirm a nearly flat noise spectrum for CheRB- cells, whereas CheRB+ cells demonstrated elevated noise at low frequencies (Fig. 4c). The amplitude of these low-frequency noise components do clearly vary from cell to cell, as can be gleaned in the diversity of single-cell power spectra. To quantify this protein-level noise due to CheR/CheB activity, we describe the fluctuating signal as an Ornstein-Uhlenbeck (O-U) process, with relaxation timescale τ and diffusion constant c, which can be interpreted as a linear-noise approximation (***Van Kampen, 1981***) to the full stochastic chemical kinetics of the network controlling the mean kinase activity a (***Emonet and Cluzel, 2008***):

$$\frac{da}{dt} = -\frac{1}{\tau}a(t) + \sqrt{c}\Gamma(t) \tag{1}$$

where $\Gamma(t)$ is a white noise process. The parameters τ and c for each cell are readily extracted via the power-spectrum solution of the O-U process:

$$S_a(\omega) = \frac{2c\tau^2}{1 + (2\pi\omega\tau)^2} + E \tag{2}$$

where we have added to the standard Lorentzian solution (***Gillespie, 1996***) a white-noise term E that may vary from cell to cell to account for experimental shot noise in the photon-limited FRET signal. Single-cell PSD data were well fit by Eq. 2 (Figure 2d), and the average of extracted single-cell fluctuation timescales ($\langle \tau \rangle = 12.6$s) (Figure 2e) are in good agreement with previously reported correlation times of flagellar motor switching (***Park et al., 2010***; ***Korobkova et al., 2004***), as well as the kinetics of CheRB-mediated changes in receptor modification from *in vivo* measurements using radioactively labeled methyl groups (***Lupas and Stock, 1989***; ***Terwilliger et al., 1986***). The noise amplitudes obtained from the fits of the PSD, $\sigma_a = \sqrt{c\tau/2}$ yielded very similar noise amplitudes as calculated from the time series ($\langle \eta_{OU} \rangle = 0.46$, see Fig. S5). Interestingly, these noise levels are larger than expected. Previous studies had predicted a value of $\sim 10 - 20\%$, based either on reported fluctuation amplitudes of motor switching (***Korobkova et al., 2004***; ***Tu and Grinstein, 2005***) or biochemical parameters of the intracellular signaling network (***Emonet and Cluzel, 2008***; ***Shimizu***

et al., 2010) and is also highly variable ($\sigma_\eta = 0.24$) from cell to cell.

In summary, we confirmed the presence of strong temporal fluctuations in single-cell chemotaxis signaling attributable to the stochastic kinetics of the adaptation enzymes CheR/CheB, and further found that the amplitude of these fluctuations vary considerably across cells in an isogenic population.

Discussion

The single-cell FRET measurements described here allowed us to quantify variability in a variety of signaling parameters of the bacterial chemotaxis system, both across cells in a population and within individual cells over time. By imaging many (up to ~ 100) cells simultaneously, we are able to collect single-cell statistics at high throughput to build up single-cell statistics. Although single-cell experiments have a long history in studies of bacterial chemotaxis (***Berg and Brown, 1972***; ***Spudich and Koshland, 1976***; ***Block et al., 1982***; ***Korobkova et al., 2004***; ***Dufour et al., 2016***), nearly all examples to date have relied on measurements of flagellar motor output (in either tethered or swimming cells). A major advantage of the FRET approach is that it provides a direct measurement of intracelluar signaling that bypasses the noisy behavior of the flagellar motor (a stochastic two-state switch), thereby enabling accurate and efficient determination of signaling parameters.

From gene-expression noise to network-level diversity

A key feature of bacterial chemotaxis as an experimental system is that one can study *in vivo* signaling and behavior in a manner that is decoupled from gene expression and growth. Being an entirely protein-based signaling network, chemotaxis signaling responses do not require changes in gene expression, and the relatively short timescales of signaling reactions (subsecond to minutes) are well separated from those of changes in protein counts due to gene expression noise (minutes to hours). The ensemble of single-cell FRET time series measured in each of our experiments thus provide a snapshot of cell-to-cell variability due to stochastic gene expression in a variety of signaling parameters.

Our data revealed high variability in important signaling parameters connected to the adaptation system (Fig. 1). In the case of the variability in recovery times (CV=0.20), this is likely due to variability in the CheR/receptor ratio from cell to cell. What consequences might such variability have on chemotactic behavior? A recent theoretical study has established that long (short) adaptation times are better suited for maximizing chemotactic migration rates in shallow (steep) gradients (***Frankel et al., 2014***). Thus, variability in adaptation times could partition the population into cells that will be more efficient in running up steep gradients, while others are specialists in climbing shallow ones. Interestingly, it was also found that optimal performance at each gradient involves tuning not only the adaptation time, but also other parameters such as swimming speed or tumble bias, leading

to a selective pressure not only for the distribution of individual parameters, but also correlations among them (***Frankel et al., 2014***; ***Waite et al., 2016***). Whether such correlated variation exists among signaling parameters would be a fruitful avenue for future single-cell FRET studies.

In the ligand response of the network, we observed large cell-to-cell variability in the sensitivity $(1/K)$ and steepness (H) of dose-response relations, for cells with a wildtype receptor population (Fig. 2). Using a mixed-species MWC model (***Mello and Tu, 2005***), we were able to estimate the Tar/Tsr ratio in single cells, which spans a broad range from nearly zero to more than two. This strong variability in the receptor-cluster composition has the potential to dramatically impact behavior. In their natural habitats, cells likely experience a variety chemoeffector gradients simultaneously, each associated with an unknown fitness payoff for chemotactic pursuit. Generating diversity in the chemoreceptor ratio, which has been shown to determine which gradient to climb when challenged with such conflicting possibilities (***Kalinin et al., 2010***), could allow the isogenic population to hedge its bets to maximize net fitness gains. The Tar/Tsr ratio has also been shown to play an important role in setting the preferred temperature for thermotaxis (***Salman and Libchaber, 2007***; ***Yoney and Salman, 2015***). Variability in Tar/Tsr would allow diversification of the preferred temperature across cells in the population, which will promote spreading of bacteria in environments with temperature gradients. Finally, when chemotactic bacteria colonize an initially nutrient-rich environment, they are known to successively exploit resources by emitting multiple traveling waves of chemotactic bacteria, each of which consumes and chases by chemotaxis a different nutrient component outward from the colony origin (***Adler, 1966***). Our observation that the population diversity in receptor ratios, and hence chemotactic preference, varies concomitantly with population growth could provide a means to tune the population fractions that engage in such excursions into virgin territory, and those that remain for subsequent exploitation of remaining resources. Thus, the diversity in ligand response and preference generated by variability in the Tar/Tsr ratio could have nontrivial consequences in a variety of behavioral contexts encountered by isogenic chemotactic (and thermotactic) populations.

Suppression of gene expression noise by CheB phosphorylation feedback

The role of phosphorylation feedback has been a long standing open question in the field of bacterial chemotaxis signaling, ever since its presumed role in providing precise adaptation was decisively ruled out by ***Alon et al.*** (***1999***). In the ensuing years, a diverse set of hypotheses have been proposed to explain its purpose. Apart from precise adaptation, CheB phosphorylation has been suggested as possibly responsible for the non-linear response of CheB activity to changes in CheA kinase activity (***Shimizu et al., 2010***; ***Clausznitzer et al., 2010***),ligand sensitivity of wild-type cells (***Barkai et al., 2001***), and as a possible mechanism to buffer gene-expression noise to suppress detrimental variability in the steady-state kinase activity. Here, we tested the latter hypothesis, by severing the phosphorylation feedback loop that has been implicated theoretically as a possible

noise-reduction mechanism (***Kollmann et al., 2005***). Our single-cell FRET data revealed that, not only does CheB phosphorylation feedback strongly attenuate the magintude of variability in the steady-state kinase activity a_0, it also qualitatively changes the shape of the distribution $P(a_0)$ across cells to convert an otherwise bimodal distribution into a unimodal one (Fig 3d). The highly polarized bimodal distribution of steady-state activities in CheB phosphorylation mutants are likely detrimental, as they could drive a_0 of a large fraction of the population too far from the flagellar motor's steep response threshold (***Cluzel et al., 2000***; ***Yuan and Berg, 2013***) to effectively control swimming. The observation of a bimodal $P(a_0)$ in the absence of phosphorylation feedback is consistent with a previous modeling study by ***Emonet and Cluzel*** (***2008***) in that the parameters of the CheR- and CheB-catalyzed covalent modification cycle appear to satisfy conditions for zero-order ultrasensitivity (***Goldbeter and Koshland, 1981***), which has been hypothesized to provide a source of slow and large amplitude temporal fluctuations with possible benefits for chemotaxis in certain environments (see below). The fact that CheB phosphorylation seems to strongly attenuate the steepness of the ultrasensitive relationship $a_0 = f([R]/[B])$ between kinase activity and the [R]/[B] ratio suggests that zero-order might not suffice to explain the large amplitude temporal fluctuations we observed in wildtype cells (see below).

Diversity in temporal noise: bet-hedging across exploration and exploitation strategies

In addition to cell-to-cell variability in signaling parameters, single-cell FRET allowed us to resolve temporal fluctuations in signaling about the steady-state output within individual cells. In wild-type cells, we found that the steady-state activity fluctuates slowly (Fig. 4,correlation time $\tau \approx 10s$) with a large amplitude ($\eta = \sigma_a/\langle a \rangle \approx 40\%$), but this amplitude also varies significantly from cell to cell ($CV \approx 0.6$). Fluctuations on this timescale were absent in CheRB- cells defective in receptor methylation/demethylation, indicating that these fluctuations are generated by stochastic processes in the activity of the adaptation enzymes CheR and CheB. Whereas the fluctuation correlation time τ in our FRET experiments was in close agreement with those from previously reported flagellar motor switching experiments (***Korobkova et al., 2004***; ***Park et al., 2010***), the fluctuation amplitude $\langle \eta \rangle \approx 40\%$ was surprisingly large. Theoretical analysis of the motor-based noise measurements (***Tu and Grinstein, 2005***) had predicted a more modest noise level of intracellular noise, at 10-20$\%$ of the mean. The discrepancy is likely due, at least in part, to the recently discovered adaptation at the level of the flagellar motor (***Yuan et al., 2012***), which must effectively act as a highpass filter that attenuates frequencies near or below a cutoff frequency determined by its own characteristic timescale for adaptation. The fluctuation amplitude η was also much greater than previous estimates from pathway-based models that considered zero-order ultrasensitivity in the enzymatic activities of CheR and CheB (***Emonet and Cluzel, 2008***) and receptor cooperativity (***Shimizu et al., 2010***) as possible sources of noise enhancement. A plausible explanation for the latter discrepancy is that

receptor cooperativity, which can amplify not only ligand signals but also fluctuations in receptor methylation levels (***Duke and Bray, 1999***; ***Shimizu et al., 2003***; ***Mello et al., 2004***), is actually much stronger at the single-cell level than estimated from previous population-level FRET measurements. The dose-response data for CheRB- cells presented in this study clearly demonstrate that single-cell dose-response curves tend to be steeper than those obtained from fits to the population average. Determining the distribution of dose-response parameters for adapting (CheRB+) cells is thus of great interest and represents a promising direction for future study.

The temporal noise we observed could have profound implications for *E. coli*'s random-walk motility strategy, because slow fluctuations in the intracellular signal can enhance the likelihood of long run events and stretch the tail of the run-length distribution to yield power-law-like switching-time distributions over a range of time scales (***Korobkova et al., 2004***; ***Tu and Grinstein, 2005***). Such non-exponential statistics are known to yield superior foraging performance in environments where resource distribution is sparse (***Viswanathan et al., 1999***), and temporal fluctuations in run-tumble behavior has also been shown theoretically to enhance climbing of shallow gradients by generating runs that are long enough to integrate over the faint gradient a detectable difference in ligand input (***Flores et al., 2012***; ***Sneddon and Emonet, 2012***). Hence, the noise generated by the adaptation system can be advantageous in resource-poor environments (*deserts*) in which efficient exploration of space for sparsely distributed sources (*oases*) is of utmost importance. By contrast, strong temporal noise clearly degrades response fidelity in rich environments where the gradient signal is strong enough for detection with short runs, and might also complicate coordination of cells in collective behaviors such as the aforementioned traveling-wave exploitation of nutrients. Our finding that the noise amplitude varies strongly from cell to cell thus suggests that isogenic populations might be hedging their bets by partitioning themselves between specialists for local exploitation of identified resource patches and those for long-range exploration in search for new ones.

Concluding remarks

We described a new single-cell FRET technique capable of resolving intracellular signaling dynamics in live bacteria over extended times. Our results highlight how a protein-based signaling network can either generate or attenuate variability, by amplifying or filtering molecular noise of different molecular origins. Gene expression noise is harnessed, on the one hand, to generate diversity in the ligand response of isogenic populations, or attenuated, on the other the hand, in the control of steady-state signal output. In addition, we showed that signaling noise generated at the level of interacting gene products, in the stochastic protein-protein interactions within the signaling network, can be amplified by the signaling network to generate strong temporal temporal fluctuations that can propagate to the level of swimming behavior.

Materials and Methods

Strains and Plasmids

All strains used are descendants of *E. coli* K-12 HCB33 (RP437). Growth conditions were kept uniform by transforming all strains with two plasmids. All strains and plasmids are shown in Tables 1 and 2.

The FRET acceptor-donor pair (CheY-mRFP and CheZ-YFP) is expressed in tandem from a IPTG inducible pTrc99A plasmid, pSJAB12 or pSJAB106, with respective induction levels of 100 and 50 μM IPTG. The differences between pSJAB12 and pSJAB106 are i) the presence of a noncoding spacer in pSJAB106 to modify the ribosome binding site of CheZ ***Salis et al.*** (***2009***), such that CheZ is expressed approximately 3 fold less, and ii) a A206K mutation in YFP to enforce monomerity. We also used pVS52 (CheZ-YFP) and pVS149 (CheY-mRFP1) to express the fusions from separate plasmids with induction levels of 50 uM IPTG and 0.01 % arabinose, respectively. We transformed the FRET plasmids in adaptation-proficient strain (VS104) to yield CheRB+ and adaptation- (VS149) to get CheRB-. For attachment with sticky flagella from pZR1 we used the equivalent strains in *fliC* background (VS115 and TSS58).

For the experiments with the CheB mutants, pSJAB12 was transformed into VS124 together with plasmids expressing $CheB^{WT}$, $CheB^{D56E}$ and truncated mutant $CheB_c$ (plasmids pVS91, pVS97 and pVS112, respectively, with induction levels of 1.5E-4, 6E-4 and 3E-4 % arabinose.

Abbreviation	Strain	Source	Relevant Genotype	plasmid 1	plasmid 2
WT / CheRB+	VS115	V. Sourjik	ΔYZ ΔFliC	pSJAB106	pZR2
WT / CheRB+	VS104	***Sourjik and Berg*** (***2002b***)	ΔCheYZ	pVS52	pVS149
WT / CheRB+	VS104		ΔCheYZ	pSJAB12	pBAD33
WT / CheRB+	VS104		ΔCheYZ	pSJAB106	pBAD33
CheRB-	TSS58	*this work*	ΔRBYZ ΔFliC	pSJAB106	pZR2
CheRB-	VS149	***Sourjik and Berg*** (***2004***)	ΔRBYZ	pVS52	pVS149
CheRB-	VS149		ΔCheRBYZ	pSJAB12	pBAD33
CheRB-	VS149		ΔCheRBYZ	pSJAB106	pBAD33
CheBc	VS124	***Clausznitzer et al.*** (***2010***)	ΔCheBYZ	pSJAB12	pVS112
D56E	VS124		ΔCheBYZ	pSJAB12	pVS97
WT CheB	VS124		ΔCheBYZ	pSJAB12	pVS91
Tsr only	UU2567	***Kitanovic et al.*** (***2015***)	ΔCheRBYZ,ΔMCP[a]	pSJAB106	pPA114 Tsr
ΔCheB	UU2614	J.S. Parkinson	CheB Δ(4-345)	pTrc99a	pVS91,97,112

All strains are descendants of E. coli K-12 HCB33 (RP437). In all FRET experiments, strains carry two plasmids and have resistance for chloramphenicol and ampicillin.

Table 1. Strains used in this study.

[a] all five chemoreceptor genes *tar tsr tap trg aer* deleted

FRET Microscopy

Föster Resonance Energy Transfer [FRET] microscopy was performed as previously reported (***Sourjijk et al., 2007***; ***Vaknin and Berg, 2004***). Cells were grown to OD=0.45-0.5 in Tryptone Broth (TB) medium from a saturated overnight culture in TB, both with 100 μg/mL ampicillin and 34 μg/mL chloramphenicol and appropriate inducers in the day culture. For the FRET experiments we used

Name	Product	System	Ind	Res	Source
pVS52	CheZ-5G-YFP	pBAD33	ara	cam	***Sourjik and Berg* (*2002b*)**
pVS149	CheY-5G-mRFP1	pTrc99a	IPTG	amp	***Sourjik and Berg* (*2002b*)**
pSJAB12	CheZ-5G-YFP / CheY-5G-mRFP1	PTrc99a	IPTG	amp	This work
pSJAB106	CheZ-5G-YFP [a] / CheY-5G-mRFP1	PTrc99a	IPTG	amp	This work
pVS91	CheB [b]	pTrc99a	ara	cam	***Liberman et al.* (*2004*)**
pVS97	CheB-D56E [c]	pBAD33	ara	cam	***Clausznitzer et al.* (*2010*)**
pVS112	CheBc [d]	pBAD33	ara	cam	V. Sourjik
pSJAB 122	CheBc-GS4G-mVenus	pBAD33	ara	cam	This work
pSJAB 123	CheB(D56E)-GS4G-mVenus	pBAD33	ara	cam	This work
pSJAB 124	CheB-GS4G-mVenus	pBAD33	ara	cam	This work
pZR 1	FliC* [e]	pKG116	NaSal	cam	This work
pPA114 Tsr	Tsr	pPA114	NaSal	cam	***Ames et al.* (*2002*)**

Table 2. Plasmids used in this study.

[a] Contains a A206K mutation to enforce monomerity.
[b] expresses WT CheB
[c] carries a point mutation D56E in CheB
[d] expresses only residues 147-349 of CheB, preceded by a start codon (Met)
[e] expresses sticky FliC element ***Scharf et al.* (*1998*)**

Motility Media (MotM) (***Shimizu et al., 2006***), in which cells do not grow and protein expression is absent. Cells were washed in 50 mL MotM, and then stored 0.5-6 h before experiment. In the dose-response curve experiments and the temporal fluctuation measurements, cells were stored up to three hours at room temperature to allow for further red fluorescence maturation.

Cells were either attached by expressing sticky FliC elements from a plasmid, with Poly-L-Lysine (Sigma), or anti FliC antibodies column purified and pre-absorbed to FliC- cells (JY26) from rabbit blood serum (a gift from Howard Berg). We found FRET experiments with sticky FliC to have the highest signal-to-noise ratio.

Fluorescent images of the cells were obtained with a magnification of 40-100x. For excitation of YFP, we either used 514 nm laser excitation set to 30 mW for 2 ms or an LED system (CoolLED, UK) with an approximate exposure time of 40 ms to approximate the same illumination intensity per frame. The sample was illuminated stroboscopically with a frequency between 1 and 0.2 Hz. RPF excitation was performed by 2ms exposure of 60 mW 568 nm laser or equivalent with LED.

Excitation light was sent through a 519 nm dichroic mirror (Semrock, USA). Epifluorescent emission was led into an Optosplit (Cairn Research, UK) with a second dichroic mirror (Semrock, USA) and two emission filters to project the RFP and YFP emission side by side on an EM-CCD (Princeton Instruments, USA) with multiplication gain 100. All devices were controlled through custom-written software.

Image processing

Images were loaded and analyzed by means of in-house written scripts in MATLAB and Python. Images were corrected for inhomogeneous illumination. Single cells were selected by image segmentation on the donor emission with appropriate filter steps to remove clusters of cells or cells improperly attached to the coverslip. At the position of each cell a rectangular ROI is defined in which all fluorescence intensity is integrated. For experiments in which the concentration of donor molecules may influence the FRET signal, the experiments on the CheB mutants, segmentation was done separately for each frame to determine the cell shape and then linking these segmented images with a tracking algorithm (***Crocker and Grier, 1996***), afterwards, fluorescence intensities are normalized for the cell size (mask surface area) in segmentation and cells with low intensities were excluded from the analysis. The ROI for the donor intensity were subsequently used to obtain the acceptor intensity per cell, both in photon-count per pixel. Fluorescence intensities were corrected for bleaching by fitting a linear, single exponential or double exponential function to the fluorescence decay, separately for both donor and acceptor. Cells in which the intensity decay cannot accurately be corrected were excluded from the analysis.

FRET analysis

The FRET signal is calculated from fluorescent time series. We observe changes in the ratio $R = A/D$, in which A and D are the fluorescence intensities of the acceptor and donor. In previous population-averaged FRET experiments the FRET per donor molecule ($\Delta D/D_0$) is calculated as (***Sourjik and Berg, 2002b***; ***Sourjijk et al., 2007***):

$$\frac{\Delta D}{D_0} = \frac{\Delta R}{\alpha + R_0 + \Delta R} \tag{3}$$

in which R_0 is the ratio in absence of FRET, $\alpha = |\Delta A/\Delta D|$ is a constant that depends on the experimental system (in our case $\alpha = 0.30$) and the change in ratio as a result of energy transfer ΔR. ΔR and R_0 are obtained through observing the ratio just after adding and removing saturated attractant stimuli. This expression is convenient because it is invariant for inhomogeneous illumination. However, in single-cell FRET this expression may generate additional variability in FRET due to variable donor levels from cell to cell. Hence it is more convenient to define the FRET levels in terms of the absolute change in donor level ΔD, since this reflects the number of resonance energy transfer pairs

$$\text{FRET}(t) = \Delta D = D_0 \frac{\Delta R}{\alpha + R_0 + \Delta R} \tag{4}$$

Since FRET occurs only when CheY-P and CheZ interact, the FRET level is proportional to the concentration of complex [Yp-Z]. If we assume the CheY-P dephosphorylation by CheZ follows Michaelis-Menten kinetics we can describe the [Yp-Z] concentration in terms of the activity of the kinase CheA. For this, we assume the system is in steady-state for timescales much larger than CheY phosphorylation-dephosphorylation cycle (≈ 100 ms). In that case, the destruction rate should

equal the rate of CheA phosphorylation and hence the FRET signal is proportional to the activity per kinase a and the amount of CheA in the kinase-receptor complex (***Sourjik and Berg, 2002b***; ***Oleksiuk et al., 2011***):

$$\text{FRET} \propto [\text{Yp-Z}] = a\frac{k_A}{k_Z}[\text{CheA}] \approx a\frac{k_A}{k_Z}[\text{CheA}]_\text{T} \tag{5}$$

This last step is only valid if we further assume CheA autophosphorylation being the rate-limiting step. This is the case only if sufficient amounts of CheZ and CheY present in the cell. We have found that the FRET level initially increases with donor (CheZ) levels, but then saturates and remains constant for CheY and CheZ (see Fig. S8).

In many cases the most relevant parameter is the normalized FRET response. The FRET level reaches maximum if all kinases are active ($a \approx 1$). In case of CheRB+ cells, this is the case when removing a saturating amount of attractant after adaptation (***Sourjik and Berg, 2002b***). For CheRB- cells the baseline activity is (***Sourjik and Berg, 2002b***; ***Shimizu et al., 2010***) close to 1. Hence the normalized FRET $\text{FRET}(t)/\text{FRET}_{\text{max}}$ represents the activity per kinase $a(t)$ and is the relevant parameter for many quantitative models for chemoreceptor activity (***Tu, 2013***).

$$a(t) = \frac{\text{FRET(t)}}{\text{FRET}_{max}} \tag{6}$$

and from $a(t)$ the steady-state activity a_0 can be determined by averaging $a(t)$ over baseline values before adding attractant stimuli.

Power Spectral Density Estimates

From FRET time series of length T and acquisition frequency f we calculated Power Spectral Density [PSD] estimates as

$$S_{\text{FRET}}(\omega) = \frac{1}{T}|\mathscr{F}(\omega)|^2 \tag{7}$$

in which $\mathscr{F}(\omega)$ is the discrete-time Fourier transform. We only consider positive frequencies and multiply by two to conserve power.

To study the influence of experimental noise and the effect of estimating τ and c from a finite time window, we generated O-U time series using the update formula (***Gillespie, 1996***)

$$X(t+\Delta t) = X(t) - \tau^{-1}\Delta t + c^{1/2}n(\Delta(t))^{1/2} \tag{8}$$

in which n denotes a sample value from a normal variable. To the generated time series Gaussian white noise was added to simulate experimental noise. The experimental noise amplitude was obtained from the average power at high frequencies.

Dose Response Curve Analysis

Normalized FRET responses to different levels of ligand are fit to a hill curve of the form

$$a = \frac{[L]^H}{[L]^H + [K]^H} \tag{9}$$

This can be connected to an MWC model of receptor cluster activity Shimizu ***Shimizu et al.*** (***2010***) in the regime $K_I << [L] << K_A$, resulting in the correspondence key

$$H = N$$

$$K = K_I e^{f_m(m)}$$

which relates the Hill slope directly to the cluster size N, and sensitivity K to the methylation energy of the receptor. We plot K on a logarithmic scale to scale linearly with energy.

To obtain expression level estimates of different receptor species we use a different MWC model. Following ***Mello and Tu*** (***2005***), we use as an expression for the normalized response of cells to ligand $[L]$ serine

$$a = \frac{\epsilon_0 \epsilon_S^{N_S} \epsilon_A^{N_A} (1 + C[L]/\tilde{K})^{N_s}}{(1 + [L]/\tilde{K})^{N_s} + \epsilon_0 \epsilon_S^{N_S} \epsilon_A^{N_A} (1 + C[L]/\tilde{K})^{N_s}} \tag{10}$$

in which N_A is the number of Tar receptors in the cluster and N_S is the number of Tsr receptors. Parameters ϵ_A, ϵ_S, ϵ_0 are the energies corresponding to binding of ligand to Tar, Tsr and the other three receptors and are the same for each cell, like C and $\tilde{K}$ which describe the disassociation constant for the active state as $K_A = \tilde{K}/C$, while N_A and N_T may vary from cell to cell. This yields the minimization problem for all 128 cells

$$\min \sum_i^{N_{cells}} \sum_j^{N_{stim}} (m_{i,j} - a_{i,j})^2 \tag{11}$$

in which $m_{i,j}$ the measured FRET response normalized to the response amplitude of cell i to stimulus L_j. This function was minimized using the matlab function fmincon (optimization toolbox). The total number $N_T = N_A + N_S$ is limited to 32. When fitting the model used the energy parameters ϵ from reference ***Mello and Tu*** (***2005***) where used as initial guess with a maximum of $\pm 5\%$ deviation. This yielded an estimate of N_A and N_S for each cell. Under the assumption that receptor clusters are well-mixed, this yields a Tar/Tsr ratio of N_A/N_S.

Parameter	Start Value ***Mello and Tu*** (***2007***)	Final Value
C	0.314	0.29
ϵ_0	0.80	0.84
ϵ_A	1.23	1.29
ϵ_S	1.54	1.61
$\tilde{K}$	–	21.2 μM

Table 3. List of global parameters used for model of Mello and Tu. In these fits, $\tilde{K}$ is a free parameter while others are constrained $\pm 5\%$ by published values.

Ultrasensitive adaptation model of phoshorylation feedback

We model the methylation-demethylation cycle of the receptors as a Goldbeter-Koshland cycle (***Goldbeter and Koshland, 1981***; ***Emonet and Cluzel, 2008***). For simplicity, we do not explicitly describe the methylation and demethylation of the receptors explicitly but instead assume that CheR (R) activates the receptor-kinase complex directly (A^*), and that CheB (B) deactivates it (A).

$$A + R \rightarrow A^* + R$$

$$A^* + B \rightarrow A + B$$

We now assume that these reactions follow Michaelis-Menten kinetics and the total amount of kinase complexes is constant ($A_T = A^* + A$). Hence the change in $\mathscr{A} = A^*/A_\mathrm{T}$ can be described as

$$\frac{d\mathscr{A}}{dt} = v_r \frac{1-\mathscr{A}}{K_r + 1 - \mathscr{A}} - v_b \frac{\mathscr{A}}{\mathscr{A} + K_b} \tag{12}$$

in which v_r and v_b are the rates for the reactions mediated by R and B, respectively. The Michaelis-Menten constants K_b and K_r are in units of A_T and are therefore dimensionless numbers. We are interested in the steady-state level $\mathscr{A}_0$ and its dependence on the kinetic parameters in equation 12. This is described by the Goldbeter-Koshland function ***Tyson et al.*** (***2003***), an exact solution to the system in case [R] and [B] are much smaller than $[A]_T$.

$$\mathscr{A}_0[v_r, v_b, K_r, K_b] = \frac{2v_r K_r}{(v_b - v_r + v_b K_b + v_r K_r + \sqrt{(v_b - v_r + v_b K_b + v_r K_r)^2 - 4(v_b - v_r)v_r K_r}} \tag{13}$$

The shape of this curve is sigmodal if the Michaelis-Menten constants K_r and K_b are much smaller than one. For CheB phosphorylation, we assume the phosphorylation rate depends linearly on active CheA and write

$$\frac{d[\mathrm{Bp}]}{dt} = k_p[\mathrm{B}]\mathscr{A}(v_r, v_b, K_b, K_r) - k_{dp}[\mathrm{Bp}] \tag{14}$$

with the corresponding conservation law B_T=B_P+B. For the case for wild-type CheB, with phosphorylation feedback, the rates can be described in terms of catalytic rate times the enzyme (subspecies) concentration

$$\begin{aligned} v_b &= k_b([\mathrm{B}_T] - [\mathrm{Bp}]) + M k_b[\mathrm{Bp}] \\ v_r &= k_r[\mathrm{R}] \end{aligned} \tag{15}$$

in which M stands for the ratio of demethylation rates of unphosphorylated and phosphorylated CheB. The fraction of the phosphorylated CheB, $[Bp]/[B]_T$, which is given by $k_{dp}/(k_p + k_{dp})$ then determines the effective activity of CheB. Equation 14 is solved numerically using Mathematica for [Bp] and the result is substituted in equation 13. In the absence of feedback, the activity can be

directly calculated from equation 13 with the rates being simply

$$v_b = k_b[\mathrm{B}]$$

$$v_r = k_r[\mathrm{R}]$$

We only need to consider the ratio of rate constants k_r and k_b which determines at which expression ratio [CheR]/[CheB] the activity equals 1/2. We assume $k_r = k_b$ for simplicity, since the shape of the curve from Eq. 13 is not affected, it only shifts the the curve along the horizontal axis. Similarly, we only consider the ratio of phosphorylation and dephosphorylation rates. This leaves the system of equations above only has a few parameters: $K_{b,r}$; M; and the ratios k_r/b_b and k_p/k_{dp}, M. In table 4, the parameters used for the calculations are listed.

We first fixed the phosphorylation rates k_p>$2k_{dp}$. This means that the steady-state phosphorylated level of CheB [B_p]/[B_T] at activity $\approx 1/3$ is around 15 %. This parameter is not constrained by any direct observation, but it is clear the system benefits from a relatively low fraction of phosphorylation, to be able to up and down regulate the levels effectively upon changes in activity.

Generally, we assume D56E to behave like unphosphorylated CheB. The gain in catalytic rate of activated CheB is estimated to be nearly a 100 fold, but this does not agree with the expression level differences between the different CheB mutants so we made a conservative estimate of 15 (the attenuating effect increases with the gain). CheBc behaves approximately like phosphorylated CheB (albeit with increase of only 7 compared to D56E), qualitatively consistent with measured *in vitro* rates for CheBc and phosphorylated intact CheB ***Anand and Stock*** (***2002***). The difference between predicted rates and might be due to the fact that the rate experiments were performed *in vitro*. Michaelis Menten constants used in the model are lower than 1, but how low is not well constrained by data, and estimations do not take into account the possible attenuating effect of phosphorylation. Our experimental data on the distribution of a_0 implies the sigmodial curve is steep in the absence of phosphorylation and hence that K_b and K_r are quite small. The variability in a_0 for CheBc is lower than D56E, implying that the curve is less steep and hence we have chosen are K_r which is not quite as low as D56E.

To simulate gene expression noise, we simulated [CheR]/[CheB] log-normal distributions with $\sigma = 0.18$ for all three strains. The mean of the distribution was chosen to yield an average steady-state network activity (a_0) of 0.4. The resulting distribution of a_0 was calculated using the corresponding Goldbeter-Koshland function for each genotype.

Parameter	Value	Literature	Source
k_r/k_p	1	0.75	***Shimizu et al.*** (***2010***)
k_{dp}/k_p	2	$k_p = 0.37^{-1}$	***Kentner and Sourjik*** (***2009***)
K_r	0.03	«1	***Emonet and Cluzel*** (***2008***)
K_b	0.03	«1	***Emonet and Cluzel*** (***2008***)
$K_b(CheBc)$	0.2	«1	
M (WT)	15	100	***Anand and Stock*** (***2002***)
M (CheBc)	7	15	***Simms et al.*** (***1985***)

Table 4. List of parameters used for Goldbeter-Koshland description of CheB phosphorylation feedback.

References

Adler J. Chemotaxis in bacteria. Science. 1966 Aug; 153(3737):708–716. http://dx.doi.org/10.1126/science.153.3737.708, doi: 10.1126/science.153.3737.708.

Alon U, Surette MG, Barkai N, Leibler S. Robustness in bacterial chemotaxis. Nature. 1999 Jan; 397(6715):168–171. http://dx.doi.org/10.1038/16483, doi: 10.1038/16483.

Ames P, Studdert CA, Reiser RH, Parkinson JS. Collaborative signaling by mixed chemoreceptor teams in Escherichia Coli. PNAS. 2002; 99:7060–65. doi: 10.1073/pnas.092071899.

Amin D, Hazelbauer G. Chemoreceptors in signalling complexes: shifted conformation and asymmetric coupling. Mol Microbiol. 2010 Dec; 78:1313–23. doi: 10.1111/j.1365-2958.2010.07408.x.

Anand GS, Stock AM. Kinetic Basis for the Stimulatory Effect of Phosphorylation on the Methylesterase Activity of CheB. Biochemistry. 2002; 41:6752–6760.

Barkai N, Alon U, Leibler S. Robust amplification in adaptive signal transduction networks. C R Acad Sci Paris, Série IV. 2001; p. 871–877.

Barkai N, Leibler S. Robustness in simple biochemical networks. Nature. 1997 Jun; 387(6636):913–917. http://dx.doi.org/10.1038/43199, doi: 10.1038/43199.

Berg HC, Brown DA. Chemotaxis in Escherichia coli analysed by Three-dimensional Tracking. Nature. 1972 Oct; 239(5374):500–504. http://dx.doi.org/10.1038/239500a0, doi: 10.1038/239500a0.

Berg HC, Tedesco PM. Transient Response to Chemotactic Stimuli in Escherichia coli. PNAS. 1975 Aug; 72(8):3235–3239. http://dx.doi.org/10.1073/pnas.72.8.3235, doi: 10.1073/pnas.72.8.3235.

Block S, Segall J, Berg H. Impulse responses in bacterial chemotaxis. Cell. 1982; 31:215–26.

Borczuk A, Staub A, Stock J. Demethylation of bacterial chemoreceptors is inhibited by attractant stimuli in the complete absence of the regulatory domain of the demethylating enzyme. Biochem Biophys Res Commun. 1986 Dec; 141:918–23.

Bray D, Levin MD, Morton-Firth CJ. Receptor clustering as a cellular mechanism to control sensitivity. Nature. 1998 05; 393(6680):85–88. http://dx.doi.org/10.1038/30018.

Celani A, Vergassola M. Nonlinearity, Fluctuations, and Response in Sensory Systems. Physical Review Letters. 2012 Jun; 108:258102+. http://dx.doi.org/10.1103/physrevlett.108.258102, doi: 10.1103/physrevlett.108.258102.

Clausznitzer D, Oleksiuk O, Løvdok L, Sourjik V, Endres RG. Chemotactic Response and Adaptation Dynamics in Escherichia Coli. PLoS Computational Biology. 2010 May; 6(5):e1000784+. http://dx.doi.org/10.1371/journal.pcbi.1000784, doi: 10.1371/journal.pcbi.1000784.

Cluzel P, Surette M, Leibler S. An Ultrasensitive Bacterial Motor Revealed by Monitoring Signaling Proteins in Single Cells. Science. 2000 Mar; 287(5458):1652–1655. http://dx.doi.org/10.1126/science.287.5458.1652, doi: 10.1126/science.287.5458.1652.

Crocker, Grien. Methods of Digital Video Microscopy for Colloidal Studies. Journal of colloid and interface science. 1996; (179):298–310.

Djordevic S, Goudreau PN, Xu Q, Stock AM, West AH. Structural basis for methylesterase CheB regulation by a phosphorylation-activated domain. PNAS. 1998 February; 95:1381–1386.

Dufour Y, Gillet S, Frankel N, Weibel D, Emonet T. Direct Correlation between Motile Behavior and Protein Abundance in Single Cells. PLoS Comput Biol. 2016; 12. doi: 10.1371/journal.pcbi.1005041.

Duke T, Bray D. Heightened sensitivity of a lattice of membrane receptors. PNAS. 1999; 96:10104–8. doi: 10.1073/pnas.96.18.10104.

Eldar A, Elowitz MB. Functional roles for noise in genetic circuits. Nature. 2010 Sep; 467(7312):167–173. http://dx.doi.org/10.1038/nature09326, doi: 10.1038/nature09326.

Elowitz MB, Levine AJ, Siggia ED, Swain PS. Stochastic Gene Expression in a Single Cell. Science. 2002 Aug; 297(5584):1183–1186. http://dx.doi.org/10.1126/science.1070919, doi: 10.1126/science.1070919.

Emonet T, Cluzel P. Relationship between cellular response and behavioral variability in bacterial chemotaxis. PNAS. 2008 Mar; 105(9):3304–3309. http://dx.doi.org/10.1073/pnas.0705463105, doi: 10.1073/pnas.0705463105.

Flores M, Shimizu TS, ten Wolde PR, Tostevin F. Signaling Noise Enhances Chemotactic Drift of *E. coli*. Physical Review Letters. 2012 Oct; 109:148101+. http://dx.doi.org/10.1103/physrevlett.109.148101, doi: 10.1103/physrevlett.109.148101.

Frankel NW, Pontius W, Dufour YS, Long J, Hernandez-Nunez L, Emonet T, Marder E. Adaptability of non-genetic diversity in bacterial chemotaxis. eLife. 2014 Oct; p. e03526+. http://dx.doi.org/10.7554/elife.03526, doi: 10.7554/elife.03526.

Gillespie DT. The mathematics of Brownian motion and Johnson noise. American Journal of Physics. 1996 March; 64:225–240.

Goldbeter A, Koshland DE. An amplified sensitivity arising from covalent modification in biological systems. PNAS. 1981 Nov; 78(11):6840–6844. http://dx.doi.org/10.1073/pnas.78.11.6840, doi: 10.1073/pnas.78.11.6840.

Kalinin Y, Neumann S, S V, Wu M. Responses of Escherichia coli bacteria to two opposing chemoattractant gradients depend on the chemoreceptor ratio. Journal of Bacteriology. 2010; 192(7):1796–1800.

Kentner D, Sourjik V. Dynamic map of protein interactions in the Escherichia Coli chemotaxis pathway. Molecular Systems Biology. 2009; .

Keymer JE, Endres RG, Skoge M, Meir Y, Wingreen NS. Chemosensing in Escherichia coli: Two regimes of two-state receptors. Proceedings of the National Academy of Sciences. 2006 Feb; 103(6):1786–1791. http://dx.doi.org/10.1073/pnas.0507438103, doi: 10.1073/pnas.0507438103.

Kitanovic S, Ames P, Parkinson JS. A Trigger Residue for Transmembrane Signaling in the Escherichia coli Serine Chemoreceptor. J Bacteriology. 2015 Aug; 197:2568–79. doi: 10.1128/JB.00274-15.

Kollmann M, Løvdok L, Bartholomé K, Timmer J, Sourjik V. Design principles of a bacterial signalling network. Nature. 2005 Nov; 438(7067):504–507. http://dx.doi.org/10.1038/nature04228, doi: 10.1038/nature04228.

Korobkova E, Emonet T, Vilar JM, Shimizu TS, Cluzel P. From molecular noise to behavioural variability in a single bacterium. Nature. 2004 Apr; 428(6982):574–578. doi: 10.1038/nature02404.

Lazova MD, Ahmed T, Bellomo D, Stocker R, Shimizu TS. Response Rescaling in Bacterial Chemotaxis. PNAS. 2011; 108(33):13870–75.

Lazova MD, Butler MT, Shimizu TS, Harshey RM. Salmonella chemoreceptors McpB and McpC mediate a repellent response to L-cystine: a potential mechanism to avoid oxidative conditions. Molecular Microbiology. 2012 May; 4(84):697–711.

Li GW, Burkhardt D, Gross C, Weissman JS. Quantifying absolute protein synthesis rates reveals principles underlying allocation of cellular resources. Cell. 2014 apr; 157(3):624–35. http://www.ncbi.nlm.nih.gov/pubmed/24766808, doi: 10.1016/j.cell.2014.02.033.

Li M, Hazelbauer GL. Cellular stoichiometry of the components of the chemotaxis signaling complex. Journal of bacteriology. 2004 Jun; 186(12):3687–3694. http://dx.doi.org/10.1128/jb.186.12.3687-3694.2004, doi: 10.1128/jb.186.12.3687-3694.2004.

Liberman L, Berg HC, Sourjik V. Effect of Chemoreceptor Modification on Assembly and Activity of the Receptor-Kinase Complex in *Escherichia Coli*. J of Bacteriology. 2004 Aug; 186(19):6643–46. doi: 10.1038/262467a0.

Lupas A, Stock J. Phosphorylation of N-terminal Regulatory Domain Activates the CheB Methylesterase in Bacterial Chemotaxis. J of Biological Chemistry. 1989 October; 264:17337–17342.

Masson JB, Voisinne G, Wong-Ng J, Celani A, Vergassola M. Noninvasive inference of the molecular chemotactic response using bacterial trajectories. PNAS. 2012 Jan; 109:1802–7. doi: 10.1073/pnas.1116772109.

Mello B, Shaw LB, Tu Y. Effects of Receptor Interaction in Bacterial Chemotaxis. Biophysical Journal. 2004 Oct; 87:1578–95.

Mello BA, Tu Y. An allosteric model for heterogeneous receptor complexes: Understanding bacterial chemotaxis responses to multiple stimuli. PNAS. 2005 Nov; 102(48):17354–17359. http://dx.doi.org/10.1073/pnas.0506961102, doi: 10.1073/pnas.0506961102.

Mello BA, Tu Y. Effects of adaptation in maintaining high sensitivity over a wide range of backgrounds for Escherichia Coli chemotaxis. Biophysical journal. 2007 Apr; 92(7):2329–2337. doi: 10.1529/biophysj.106.097808.

Mesibov R, Ordal GW, Adler J. The Range of Attractant Concentrations for Bacterial Chemotaxis and the Threshold and Size of Response over This Range. The Journal of General Physiology. 1973; 62(2):203–223. http://jgp.rupress.org/content/62/2/203, doi: 10.1085/jgp.62.2.203.

Min TL, Mears PJ, Golding I, Chemla YR. Chemotactic adaptation kinetics of individual Escherichia Coli cells. PNAS. 2012 june; .

Neumann S, Vladimirov N, Krembel AK, Wingreen NS, Sourjik V. Imprecision of adaptation in Escherichia Coli chemotaxis. PLoS ONE. 2014; 9(1):1–6.

Oleksiuk O, Jakovljevic V, Vladimirov N, Carvalho R, Paster E, Ryu WS, Meir Y, Wingreen NS, Kollmann M, Sourjik V. Thermal Robustness of Signaling in Bacterial Chemotaxis. Cell. 2011 Apr; 145(2):312–321.

Ozbudak EM, Thattai M, Kurtser I, Grossman AD, Van Oudenaarden A. Regulation of noise in the expression of a single gene. Nature genetics. 2002 May; 31(1):69–73. doi: 10.1038/ng869.

Park H, Pontius W, Guet CC, Marko JF, Emonet T, Cluzel P. Interdependence of behavioural variability and response to small stimuli in bacteria. Nature. 2010 Dec; 468(7325):819–823. http://dx.doi.org/10.1038/nature09551, doi: 10.1038/nature09551.

779 **Parkinson JS**, Hazelbauer GL, Falke JJ. Signaling and sensory adaptation in Escherichia Coli chemoreceptors:
780 2015 update. Trends in Microbiology. 2015; 23(5):257–266. http://dx.doi.org/10.1016/j.tim.2015.03.003.

781 **Raj**, Van Oudenaarden A. Nature, nurture, or chance: stochastic gene expression and its consequences.
782 Cell. 2008 oct; 135(2):216–26. http://www.pubmedcentral.nih.gov/articlerender.fcgi?artid=3118044{&}tool=
783 pmcentrez{&}rendertype=abstract, doi: 10.1016/j.cell.2008.09.050.

784 **Rao C**, Wolf DM, Arkin AP. Control, exploitation and tolerance of intracellular noise. Nature. 2002 11;
785 420(6912):231–237. http://dx.doi.org/10.1038/nature01258.

786 **Raser JM**, O'Shea EK. Control of Stochasticity in Eukaryotic Gene Expression. Science. 2004; 304:1811–14. doi:
787 10.1126/science.1098641.

788 **Salis HM**, Mirsky EA, Voigt CA. Automated design of synthetic ribosome binding sites to control protein
789 expression. Nature Biotechnology. 2009; .

790 **Salman H**, Libchaber A. A concentration-dependent switch in the bacterial response to temperature. Nature
791 Cell Biology. 2007; 9(9):1098–1100. doi: 10.1038/ncb1632.

792 **Scharf BE**, Fahrner KA, Turner L, Berg HC. Control of direction of flagellar rotation in bacterial chemotaxis. PNAS.
793 1998; 95:201–206.

794 **Segall JE**, Block SM, Berg HC. Temporal Comparisons in Bacterial Chemotaxis. PNAS. 1986; p. 8987–8991.

795 **Shimizu TS**, Aksenov SV, Bray D. A spatially extended stochastic model of the bacterial chemotaxis signalling
796 pathway. Journal of molecular biology. 2003 May; 329(2):291–309. http://view.ncbi.nlm.nih.gov/pubmed/
797 12758077.

798 **Shimizu TS**, Tu Y, Berg HC. A modular gradient-sensing network for chemotaxis in Escherichia coli revealed by
799 responses to time-varying stimuli. Molecular Systems Biology. 2010 Jun; 6. http://dx.doi.org/10.1038/msb.
800 2010.37, doi: 10.1038/msb.2010.37.

801 **Shimizu TS**, Delalez N, Pichler K, Berg HC. Monitoring bacterial chemotaxis by using bioluminescence resonance
802 energy transfer: absence of feedback from the flagellar motors. PNAS. 2006; .

803 **Simms SA**, Keane MG, Stock J. Multiple forms of the CheB methylesterase in Bacterial Chemosensing. J of
804 Biological Chemistry. 1985 August; 260:10161–10168.

805 **Sneddon MW**, Emonet T. Modeling cellular signaling: taking space into the computation. Nat Meth. 2012 Mar;
806 9(3):239–242. doi: 10.1038/nmeth.1900.

807 **Sourjijk V**, Vaknin A, Shimizu TS, Berg HC. In vivo measurement by FRET of pathway activity in bacterial
808 chemotaxis. Methods Enzymology. 2007; (423):365–91.

809 **Sourjik V**, Berg HC. Binding of the Escherichia coli response regulator CheY to its target measured in vivo by
810 fluorescence resonance energy transfer. PNAS. 2002 Oct; 99(20):12669–12674. http://dx.doi.org/10.1073/
811 pnas.192463199, doi: 10.1073/pnas.192463199.

812 **Sourjik V**, Berg HC. Receptor sensitivity in bacterial chemotaxis. PNAS. 2002 Jan; 99(1):123–127. http://dx.doi.
813 org/10.1073/pnas.011589998, doi: 10.1073/pnas.011589998.

814 **Sourjik V**, Berg HC. Functional interactions between receptors in bacterial chemotaxis. Nature. 2004 Mar;
815 428(6981):437–441. http://dx.doi.org/10.1038/nature02406, doi: 10.1038/nature02406.

816 **Spudich JL**, Koshland DE. Non-genetic individuality: chance in the single cell. Nature. 1976 Aug; 262(5568):467–
817 471. http://dx.doi.org/10.1038/262467a0, doi: 10.1038/262467a0.

818 **Stewart RC**. Activating and inhibitory mutations in the regulatory domain of CheB, the methylesterase in
819 bacterial chemotaxis. J of Biological Chemistry. 1993 January; 268:1921–1930.

820 **Stewart RC**, Roth AF, Dahlquist FW. Mutations that affect control of the methylesterase activity of CheB, a
821 component of the chemotaxis adaptation system in E. Coli. J of Bacteriology. 1990 June; 172:3388–3399.

822 **Taniguchi Y**, Choi PJ, Li GW, Chen H, Babu M, Hearn J, Emili A, Xie XS. Quantifying E. Coli Proteome and
823 Transcriptome with Single-Molecule Sensitivity in Single Cells. Science. 2010; 329(5991):533–539. http:
824 //www.pubmedcentral.nih.gov/articlerender.fcgi?artid=2922915{&}tool=pmcentrez{&}rendertype=abstract.

825 **Taylor BL**, Koshland DE. Electron taxis and blue light effect on bacterial chemotaxis. Journal of Bacteriology.
826 1975; 123:557–569.

827 **Taylor BL**, Miller JB, Warrick HM, Koshland DE. Electron acceptor taxis and blue light effect on bacterial
828 chemotaxis. Journal of Bacteriology. 1979; 140:567–573.

829 **Terwilliger T**, Wang J, Koshland D. Kinetics of Receptor Modification. Journal of Biol Chemistry. 1986; 261:10814–
830 20.

831 **Tu Y**. Quantitative Modeling of Bacterial Chemotaxis: Signal Amplification and Accurate Adaptation. Annual
832 Review of Biophysics. 2013 February; 42:337–359.

833 **Tu Y**, Shimizu TS, Berg HC. Modeling the chemotactic response of Escherichia coli to time-varying stimuli. PNAS.
834 2008 Sep; 105(39):14855–14860. http://dx.doi.org/10.1073/pnas.0807569105, doi: 10.1073/pnas.0807569105.

835 **Tu Y**, Grinstein G. How White Noise Generates Power-Law Switching in Bacterial Flagellar Motors. Phys
836 Rev Lett. 2005 May; 94:208101. http://link.aps.org/doi/10.1103/PhysRevLett.94.208101, doi: 10.1103/Phys-
837 RevLett.94.208101.

838 **Tyson JJ**, Chen KC, Novak B. Sniffers, buzzers, toggles and blinkers: dynamics of regulatory and signaling
839 pathways in the cell. Current Opinion in Cell Biology. 2003 Apr; 15(2):221–231. http://view.ncbi.nlm.nih.gov/
840 pubmed/12648679.

841 **Vaknin A**, Berg HC. Single Cell FRET imaging of phosphatase activity in the Escherichia coli chemotaxis system.
842 PNAS. 2004 Dec; 101(49):170272–7.

843 **Van Kampen NG**. Stochastic Processes in Physics and Chemistry. Elsevier Science; 1981. http://www.amazon.
844 com/exec/obidos/redirect?tag=citeulike07-20&path=ASIN/0444866507.

845 **Viswanathan G**, Buldyrev S, Havlin S, da Luz MGE, Raposo E, Stanley HE. Optimizing the success of random
846 searches. Nature. 1999; 401:911–914. doi: 10.1038/44831.

847 **Wadhams GH**, Armitage JP. Making sense of it all: bacterial chemotaxis. Nature Reviews Molecular Cell Biology.
848 2004 Dec; 5(12):1024–1037. doi: 10.1038/nrm1524.

849 **Waite AJ**, Frankel NW, Dufour YS, Johnston JF, Long J, Emonet T. Non-genetic diversity modulates population
850 performance. Molecular Systems Biology. 2016; 12.

851 **Wright S**, Walia B, Parkinson JS, Khan S. Differential activation of Escherichia coli chemoreceptors by blue-light
852 stimuli. Journal of bacteriology. 2006 Jun; 188(11):3962–3971.

853 **Yang Y**, Pollard AM, Höfler C, Gernot Poschet G, Wirtz R M andHell, Sourjik V. Relation between chemotaxis and
854 consumption of Amino Acids in bacteria. Molecular Microbiology. 2015; 96:1272–1282.

855 **Yoney A**, Salman H. Precision and Variability in Bacterial Temperature Sensing. Biophysical Journal. 2015;
856 108(May).

857 **Yuan J**, Berg H. Ultrasensitivity of an adaptive bacterial motor. J Mol Biol. 2013 May; 425:1760–4. doi:
858 10.1016/j.jmb.2013.02.016.

859 **Yuan J**, Branch RW, Hosu BG, Berg HC. Adaptation at the output of the chemotaxis signalling pathway. Nature.
860 2012 Apr; 484(7393):233–236. http://dx.doi.org/10.1038/nature10964, doi: 10.1038/nature10964.

Acknowledgments

We thank Simone Boskamp for cell culture, Marco Kamp for microscopy assistance and Marco Konijnenburg, Luc Blom and Eric Clay for software and electronic support. We also thank Pieter de Haan and Istvan Kleijn for help with initial measurements and William Pontius for useful discussions. We thank Sandy Parkinson and Germán Piñas for many useful discussion and a critical reading of the manuscript.

Competing interests

The authors declare they have no financial or non-financial competing interests.

869 ## Main Figures

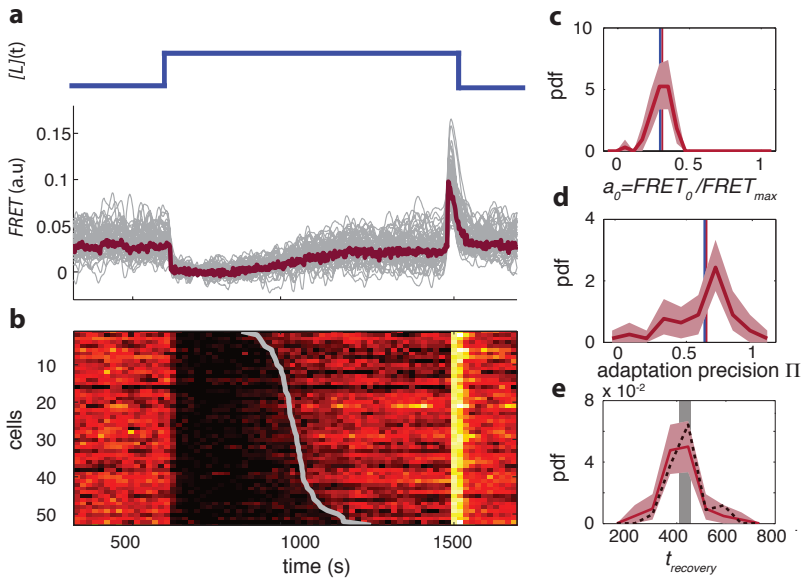

Figure 1. Single-cell FRET over extended times reveals cell-to-cell variability in signaling response. **(a)** Step-response experiment on wildtype cells (CheRB+; VS115). (Top) The ligand time series $[L](t)$ indicates the applied temporal protocol for addition and removal of 500 μM MeAsp. (Bottom) FRET response of 54 cells (grey) with the ensemble-averaged time series (dark red) overlaid. Single-cell time series were lowpass filtered with a 14s moving-average filter. **(B)** Heatmap representation of the normalized FRET response time series, with each row representing a single cell, and successive columns representing the 10s time bins in which the color-indicated activity was computed from the FRET time series. Activity was computed by normalizing FRET to the total response amplitude (Max-Min for each time series). Rows are sorted by the corresponding cell's recovery time (grey curve), defined as the time at which the activity recovered to 50 % of the activity level after adaptation (see panel e). **(c)** Steady-state activity a_0 of the cells shown in panels (a-b). Also shown are the mean steady-state activity (red vertical line) and the steady-state activity of the population averaged time series (blue vertical line). **(d)** Adaptation precision Π obtained from the FRET data. An adaptation precision of 1 denotes perfect adaptation. Also shown are the mean precision (red vertical line) and the precision of the population averaged time series (blue vertical line). The mean and std of the distribution is 0.79 ± 0.32. All colored shaded areas refer to 95 % confidence intervals obtained through bootstrapping. **(e)** Recovery time of cells defined as recovery to 50% of the post-adaptational activity level (red, 54 cells) or 50% of pre-stimulus activity (black dashed, 44 cells with precision >0.5) and simulated effect of experimental noise for a population with identical recovery times (grey). The latter was obtained from a simulated data set in which 55 time series were generated as described in Fig. S2. The width of the bar is defined by the mean plus (minus) the std of the simulated distribution. The mean and std of the distributions for the experimental and simulated data sets are respectively 416 ± 83 and 407 ± 35.

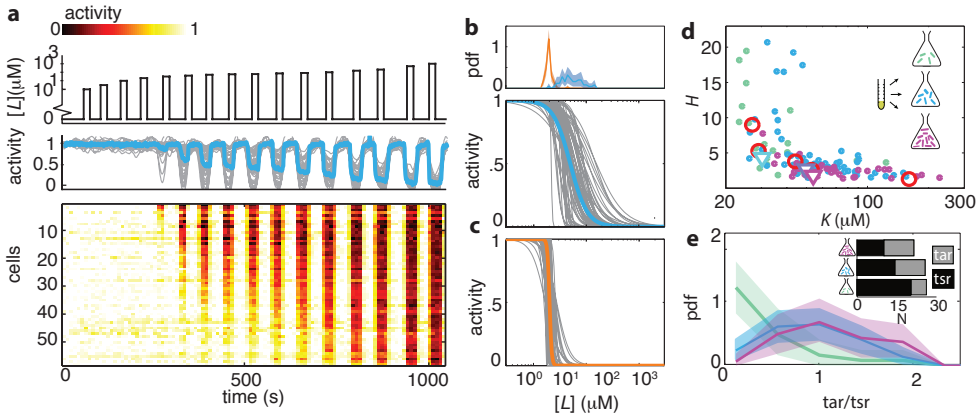

Figure 2. Ligand dose-response parameters vary strongly across cells in an isogenic population, even in the absence of adaptation. **(a)** Single-cell dose-response experiment on adaptation deficient (CheRB-; TSS58) cells with a wildtype complement of receptors. (Top) Temporal protocol of stimulation $[L](t)$ by the attractant L-serine. (Middle) The ensemble-averaged FRET response of the population (blue) and single cells (gray) in signaling activity of 59 cells, normalized to the full-scale FRET response amplitude. (Bottom) Heatmap representation of the single-cell FRET timeseries, with the rows sorted by the sensitivity K of the corresponding cell obtained from Hill-curve fits. **(b)** Family of dose response curves (gray) obtained from the Hill-curve fits to single-cell dose-response data. CheRB- cells with a wildtype complement of receptors (TSS58). The blue curve was obtained from fitting a hill function to the population-averaged time series shown in panel (a), yielding fit values K=50 μM and H=2.7. The fitted single-cell K values are shown in the histogram on top (blue). **(c)** CheRB- cells expressing only the serine receptor Tsr (UU2567). The orange curve was obtained from fits to the population average, yielding K=20 μM and H=22. The fitted single-cell K values are shown in the histogram in panel (b) (orange). textbf(d) Cells from a single overnight culture were innoculated into three flasks harvested at different times during batch-culture growth growth to sample the state of the population at three points along the growth curve: at OD_{600}=0.31 (green), 0.45 (blue) and 0.59 (purple). Hill-curve sensitivity K and cooperativity H obtained from fits to the single-cell time series, at different OD's. Shown are 25 out of 28 cells harvested at OD=0.31, 59 out of 64 cells at OD=0.45, 34 out of 40 cells at OD=0.59. The excluded cells had a mean squared error higher then 0.05. **e)** Histograms of Tar/Tsr ratio obtained from fit of multi-species MWC model from reference ***Mello and Tu*** (***2005***) to single-cell FRET time series. The mean Tar/Tsr ratios (low to high OD) are 0.4, 0.9, and 1.2 with coefficients of variance of respectively 1.1, 0.5, and 0.4. Inset: average cluster size of Tar (grey) and Tsr (black) at different harvesting OD's obtained from the fit results in panel d.

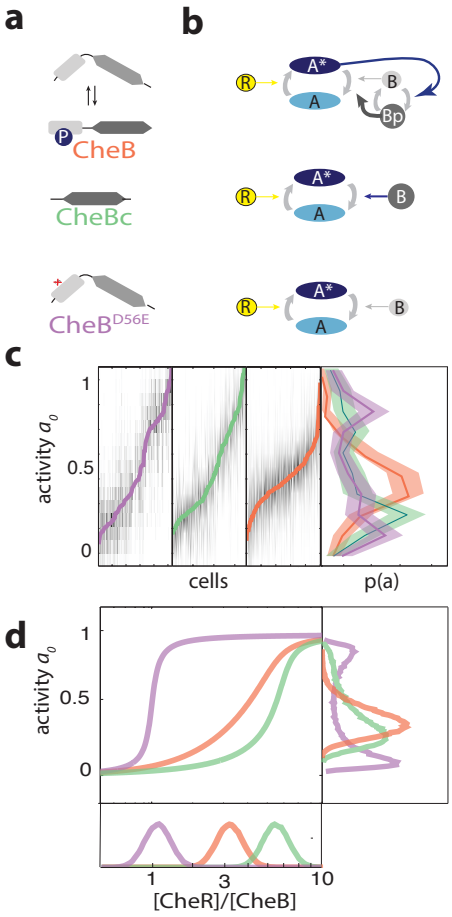

Figure 3. CheB phosphorylation feedback attenuates variability in steady-state kinase activity. **(a)** Schematic depiction of CheB activation by phosphorylation. (Top) CheB consists of two domains connected by a flexible linker. The aspartate at residue 56 can be phosphorylated. (Middle) CheBc lacks the receiver domain with the phosphorylation site. (Bottom) CheB-D56E carries a point mutation at the phosphorylation site. **(b)** Effective network topology of cells expressing WT CheB (top), CheBc (middle) and CheB-D56E (bottom). **(c)** Heatmaps showing distributions of activity a(t) of one cell (normalized to Max-Min for each time series) in each column for each CheB mutant in a *cheB* background (VS124, colors as in panel (a)) with the steady-state activity a_0 superimposed. (right) Histograms with a_0 for each CheB mutant. All histograms contain the results for cells with a signal-to-noise ratio higher than 1, which corresponds to 322 out of 373 cells (WT), 225 out of 279 cells (CheBc) and 226 out of 359 cells (D56E). Shaded regions represent bootstrapped 95% confidence intervals. **(d)** A simple kinetic model of the chemotaxis network illustrates the crucial role of CheB phosphorylation feedback in circumventing detrimental bimodality in a_0. Due to saturated enzyme kinetics in the adaptation system, the transfer function between [CheR]/[CheB] expression ratio and steady-state network output a_0 can be highly nonlinear (main panel). The shape of this transfer function determines the distribution of a_0 (right panel) by transforming the distribution of [CheR]/[CheB] expression ratios (bottom panel). Shown are a CheB version with lower activity as WT (purple) and higher than WT (green), both without feedback, and one CheB species with phosphorylation feedback (orange).

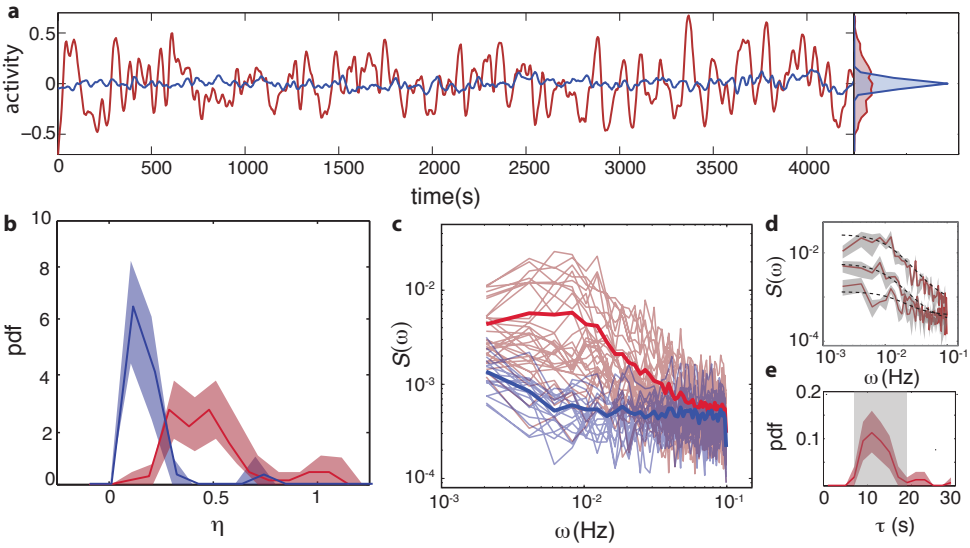

Figure 4. Temporal signal fluctuations in the absence of ligand stimulation are generated by stochastic activity of the adaptation enzymes CheR/CheB. **(a)** Representative single-cell FRET time series of steady-state fluctuations in the presence (CheRB+, VS115, red) and absence (RB-,TSS58,blue) of adaptation kinetics in normalized activity units. **(b)** Histogram of fluctuation amplitude η for both CheRB+ (70 cells, red) and CheRB- (33 cells, blue), extracted from calculating the standard deviation of a low-pass filtered FRET time series over a 10s window divided by the mean FRET level of a single cell. The shaded areas represents the 95% confidence interval obtained from bootstrapping. **(c)** Power spectral density (PSD) computed from single-cell FRET time series of 31 CheRB+ cells (red) and 17 CheRB- cells (blue), each from a single experiment. Thin curves in the lighter shade of each color represent Single-cell spectra, and the thick curves in the darker shade are the average of all single-cell spectra for each genotype. **(d)** Representative single-cell PSDs and fits by an Ornstein-Uhlenbeck (O-U) process. Shown are O-U fits (Lorentzian with constant noise floor; dashed curves) to three single-cell PSDs (solid curves). The shaded area represents the standard error of the mean for PSDs computed from nine non-overlapping segments of each single-cell time series. **(e)** Histogram of fluctuation timescales τ extracted from single-cell PSD fits (red, 70 cells from three independent experiments). The shaded areas represents the 95% confidence interval obtained from bootstrapping. The grey shaded area refers to the variability (mean±std) that can be explained by experimental noise and a finite time window, obtained through simulated O-U time series (see Materials and Methods)

870 # Supplemental Information

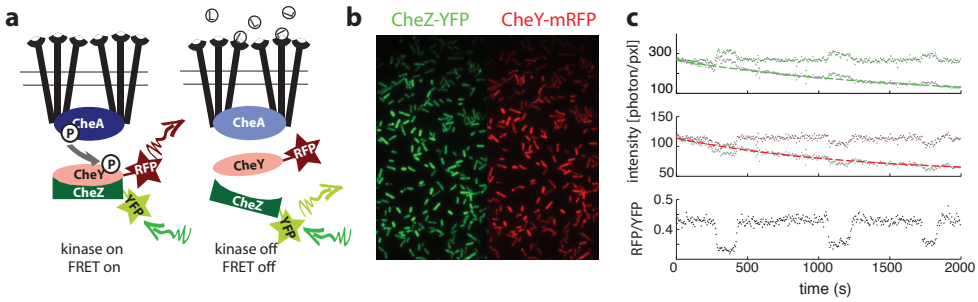

Figure S1. a) Schematic of FRET assay to measure *in vivo* kinase activity. In absence of ligand stimuli, receptors are activating CheA. When active, CheA phosphorylates CheY, increasing interaction between CheY and phosphatase CheZ and thereby increasing FRET through the labeled fluorophores. Ligand-receptor binding shuts down the kinase, which ceases phosphate transfer and FRET levels decrease. **b)** False-color images of donor (CheZ-YFP) and acceptor (CheY-mRFP1) fluorescence, channels projected on the same EM-CCD camera chip. **c)** Example time series fluorescence from a single cell (CheRB-,VS149/pVS149/52). In grey raw data is shown, with a fit to a single exponential function with offset overlaid for donor (top, green) and acceptor channel (middle, red). From the corrected fluorescence intensities the ratio RFP/YFP is calculated (bottom).

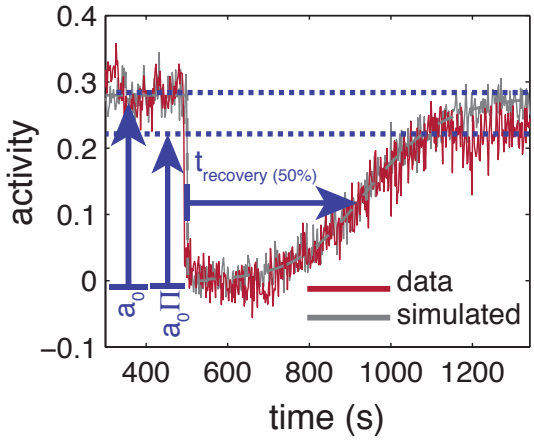

Figure S2. Cell-to-cell variability in recovery times and steady-state activity. **(a)** Simulated time series for are calculated by integrating the linearized MWC model with adaptation kinetics (***Tu et al., 2008***) with parameters chosen to closely approximate the population averaged response (grey-dashed line). To the simulated time series of each cell gaussian white noise $(\mu = 0; \sigma = 0.15)$ is added to approximate the noise level of the experiment. Also shown are the baseline and recovery levels (blue dashed lines) of the experimental population.

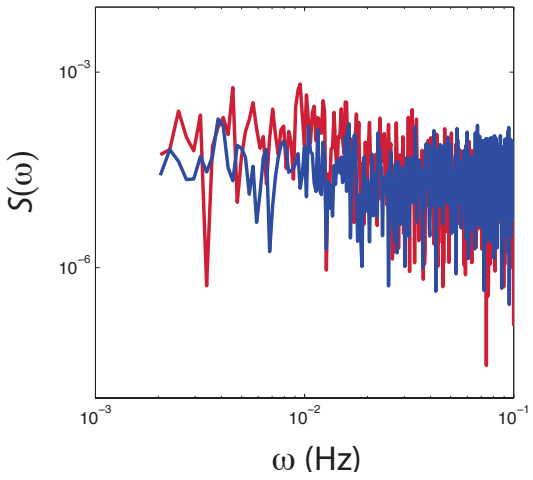

Figure S3. Power spectral density estimates from population averaged time series of CheRB+ (red) and CheRB- cells (blue). The time series are from the same experiment as shown in Figure 3b

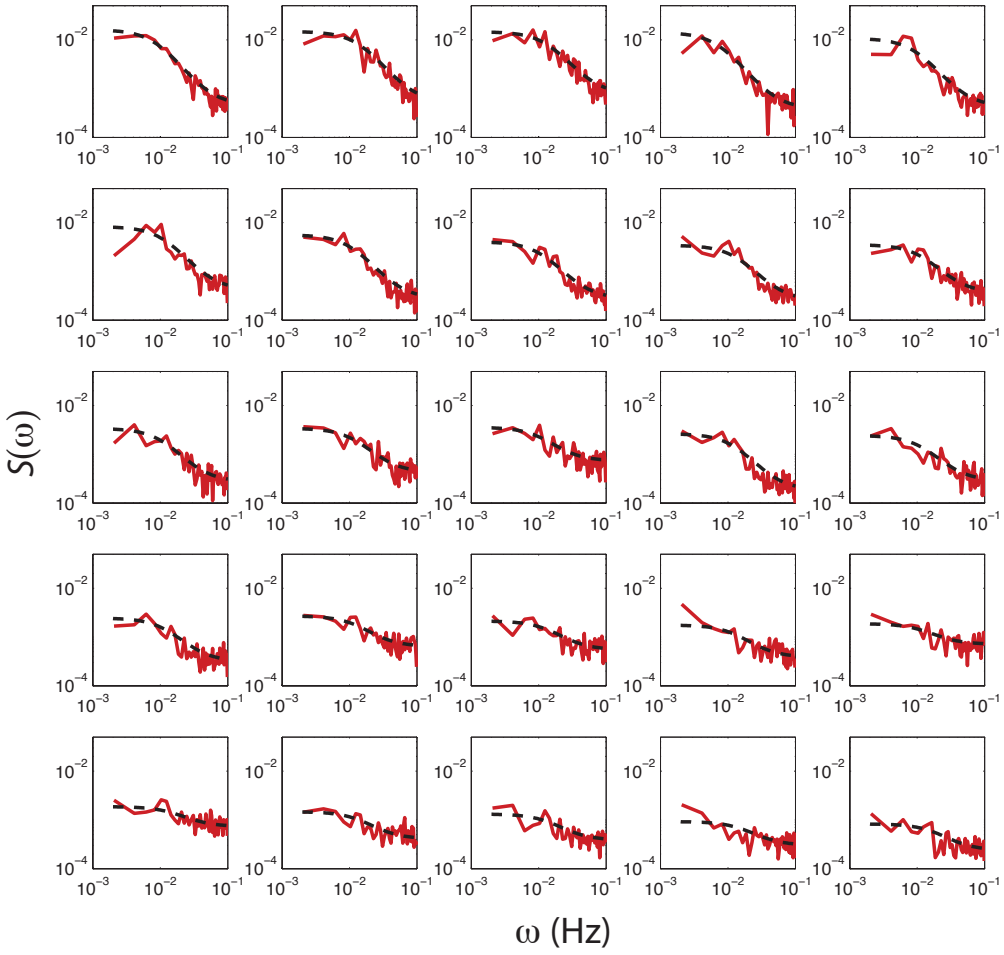

Figure S4. PSD estimates obtained from single-cell FRET time series (red dashed curve) with fits of O-U process to PSD estimates to 25 out of 31 cells (black dashed curve) from a single experiment shown in Figure 3b. The cells are sorted by variance calculated from the fit ($c\tau/2$), with top-left having the highest. The excluded cells could not properly be fit because the low frequency noise did not exceed the experimental noise floor, defined as lower than 5 times the standard deviation of the noise floor.

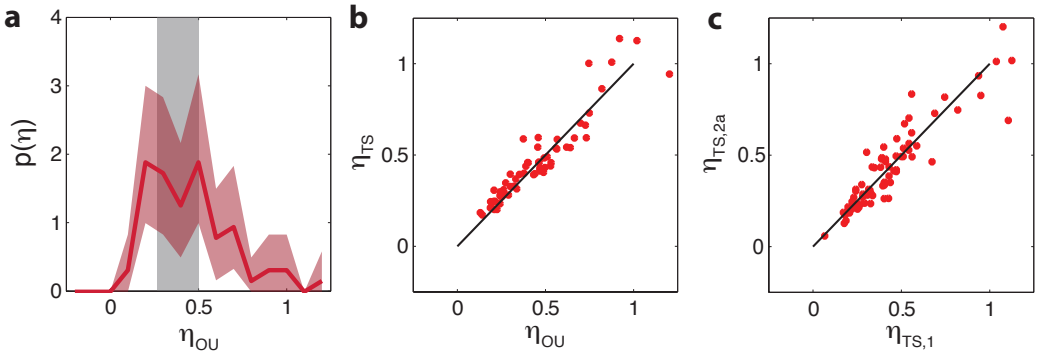

Figure S5. a Noise amplitude η_{OU} for 70 CheRB+ cells time series (from 3 experiments) obtained with mean noise level of 0.42. The grey shaded area indicates the expected noise amplitude variability based on a finite time window and experimental noise in the experiment. The width is defined as the mean plus (minus) one standard deviation of the distribution of noise amplitudes obtained from simulated OU timeseries. **b** Noise amplitude η_{OU} obtained from fits of Ornstein-Uhlenbeck process to power spectra versus the noise amplitude η_{TS} obtained through calculating the standard deviation of the FRET time series after 10s average filtering. Also shown is the diagonal $\eta_{OU} = \eta_{TS}$. **c** The noise amplitude of the first ($\eta_{TS,1}$) and second half ($\eta_{TS,2}$) of the time series show high correlation. All noise amplitudes are as coefficient of variance.

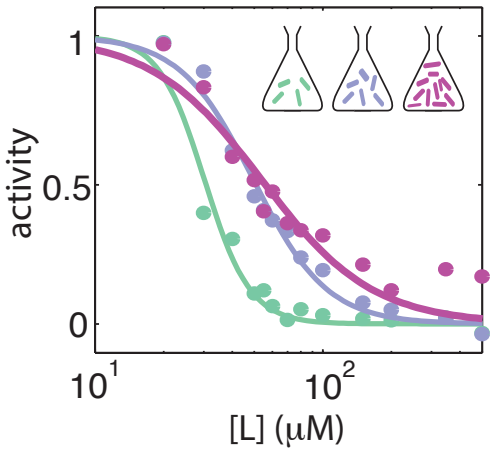

Figure S6. Dose response curves from population-averaged time series at harvesting OD's 0.31 (green), 0.45 (blue) and 0.59 (purple). The K/H fit value pairs are respectively 30/4.3, 50 /2.7 and 53/1.8.

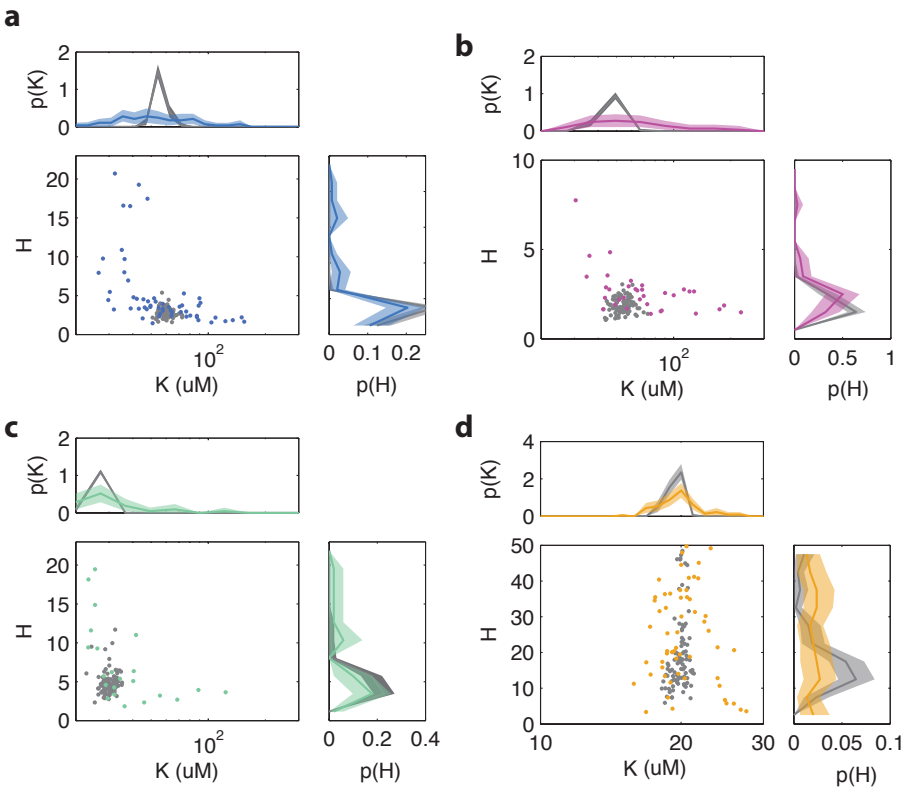

Figure S7. Distributions of fit parameters K and H from Hill curve fits to single-cell dose-response experiment. Colored points and lines indicate fits to measurement data, gray lines and points are from a simulation in which gaussian white noise is added to a dose response curve with K and H obtained from a fit to the population averaged time series. The noise level of the simulation is chosen such to approximate the average mean-squared error [MSE] of the dose response curve fits. Experimental data with a MSE exceeding a determined threshold are removed from the analysis. For the experiment on cells with WT receptor complement (TSS58) a maximum mse of 0.05 is used, excluding 5 cells for **(b)** for the experiment at OD=0.45, this excludes 5 cells, at **(d)** OD=0.31, 3 cells and at **(c)** OD=0.59, 6 cells. **(d)** For the experiment on Tsr-WT (UU2567) 11 cells are removed by the same criterion. All shaded areas indicate 95 % confidence intervals obtained through bootstrapping.

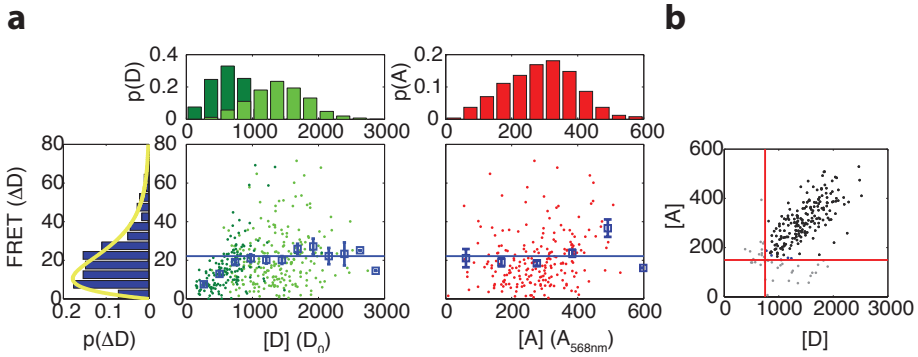

Figure S8. Relation between maximum FRET response and CheY / CheZ expression levels. **a)** (Left) Scatter plot with donor intensity (D_0, green) versus FRET response (ΔD) and (right) acceptor intensity (A, red, measured by direct excitation) with marginal distributions for A, D and ΔD in VS104/pSJAB12. For the donor intensity we measured at low induction (10 μM IPTG, dark green) and high induction (100 μM IPTG, light green). The acceptor intensities were only measured at high induction. In the scatter plots the mean FRET response is plotted with the error bars (blue), the horizontal line indicating the average for the binned data as described in panel B. The distribution of the FRET response (extreme left) is only for the gated data. The yellow curve is a fit to a gamma distribution with corresponding values and 95% confidence intervals of $k = 2.0 \pm 0.4$ and $\theta = 10.2 \pm 2.5$. All fluorescent intensities are measured in photons/pixel. All histograms are normalized to the number of cells. **b)** Gating of the data. Scatter plot of donor intensity versus acceptor intensity. All data with fluorescent intensities (in photons/pixel) lower than D=750 or A=175 are excluded from the analysis since the FRET response may be limited by the expression of either CheZ or CheY.

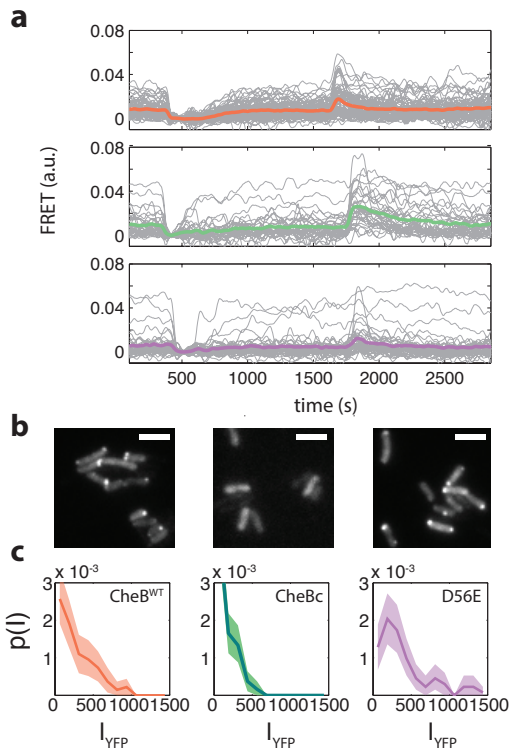

Figure S9. a Example time FRET time series for cells expressing CheB^{WT} (top, pink), CheB^{D56E} (blue, right) , CheB$_c$ (green, right) in ΔCheB (VS124) background. **b** Spatial organisation of CheB in the cell probed by mVenus fusions to CheB. Clustering was quantified by the fraction of cells clearly showing one or more clusters in the cell. Shown are representative examples of CheB^{WT} (left, 78% clustered), CheB$_c$ (middle, 0%), CheB^{D56E} (right, 72%). Scale bars 2 μm. **c** Histograms fluorescence intensity below in units of photons/pixel. Mean and standard deviation of these distributions for the strains is (from left to right) 272 ± 237 (114 cells), 148 ± 133 (150 cells) and 398 ± 328 (106 cells). This corresponds to std/mean 0.87, 0.90, 0.82 for the different CheB genotypes.

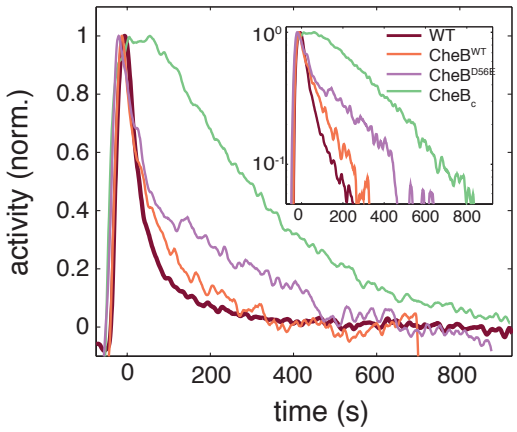

Figure S10. Phosphorylation feedback is not a necessary condition for highly non-linear adaptation dynamics. Population FRET time series of cells expressing $CheB^{WT}$ (orange), $CheB^{D56E}$ (purple) , $CheB_c$ (green) in ΔCheB (VS124) background as well as WT (CheB from native chromosome position, VS104, brown) are shown after removal of 500 μM to which cells have adapted. The strain expressing $CheB^{D56E}$ lacks phosphorylation feedback but has a fast, non-linear removal response. The population FRET experiment is performed as described previously (***Sourjik and Berg, 2002b***). The strains and induction levels are the same as in the single-cell FRET experiments on the CheB mutants.

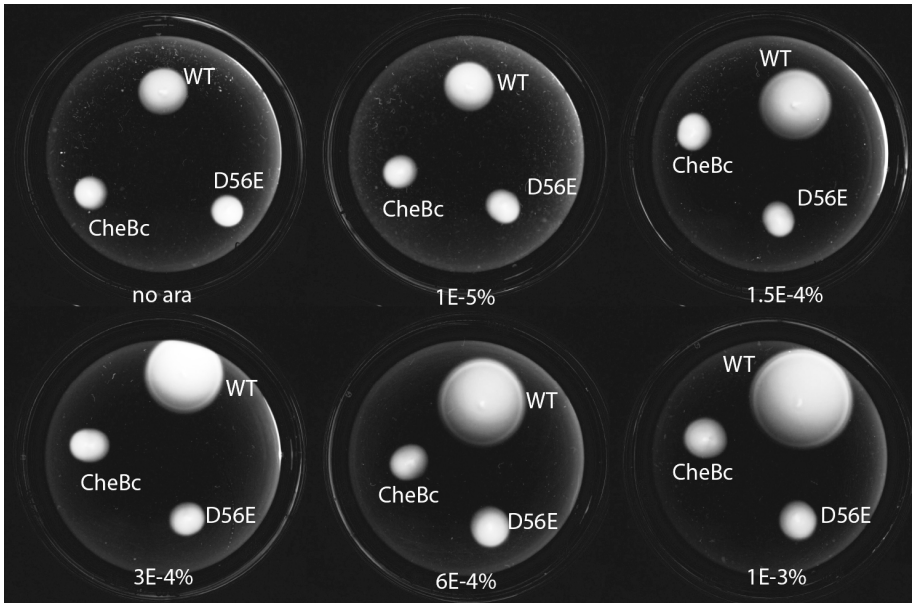

Figure S11. Dark-field images after 14 h of growth and motility on soft agar plates (0.26 % agar in TB with appropriate antibiotics, kept at 33.5 ° C). The different strains express either WT CheB, CheB-D56E and CheBc from an arabinose inducable pBAD plasmid in Δ CheB strain (UU2614). The arabinose concentration is varied from 0 % to 0.001 %